

# Regulatory T cells crosstalk with tumor cells and endothelium through lymphotoxin signaling

Received: 5 March 2024

Accepted: 25 November 2024

Published online: 02 December 2024

 Check for updates

Wenji Piao<sup>1,2,10</sup>  , Long Wu<sup>1,2,10</sup>, Yanbao Xiong<sup>1,2,10</sup>, Gregory C. Zapas<sup>2,10</sup>, Christina M. Paluskiewicz<sup>1</sup>, Robert S. Oakes<sup>3</sup>, Sarah M. Pettit<sup>2</sup>, Margaret L. Sleeth<sup>4</sup>, Keli L. Hippen<sup>4</sup>, Jessica Schmitz<sup>5</sup>, Philipp Ivanyi<sup>6</sup>, Amol C. Shetty<sup>7</sup>, Yang Song<sup>7</sup>, Dejun Kong<sup>2</sup>, Young Lee<sup>1,2</sup>, Lushen Li<sup>1,2</sup>, Marina W. Shirkey<sup>2</sup>, Allison Kensiski<sup>10</sup>, Aamna Alvi<sup>2</sup>, Kevin Ho<sup>2</sup>, Vikas Saxena<sup>10</sup>, Jan H. Bräsen<sup>5</sup>, Christopher M. Jewell<sup>3</sup>, Bruce R. Blazar<sup>4</sup>, Reza Abdi<sup>8</sup> & Jonathan S. Bromberg<sup>1,2,3,9</sup>  

Regulatory T cells (Tregs) with multifaceted functions suppress anti-tumor immunity by signaling surrounding cells. Here we report Tregs use the surface lymphotoxin (LT) $\alpha$ 1 $\beta$ 2 to preferentially stimulate LT beta receptor (LT $\beta$ R) nonclassical NF $\kappa$ B signaling on both tumor cells and lymphatic endothelial cells (LECs) to accelerate tumor growth and metastasis. Selectively targeting LT $\beta$ R nonclassical NF $\kappa$ B pathway inhibits tumor growth and migration in vitro. Leveraging in vivo Treg LT $\alpha$ 1 $\beta$ 2 interactions with LT $\beta$ R on tumor cells and LECs, transfer of wild type but not LT $\alpha$ <sup>-/-</sup> Tregs promotes B16F10 melanoma growth and tumor cell-derived chemokines in LT $\beta$ R<sup>-/-</sup> mice; and increases SOX18 and FLRT2 in lymphatic vessels of LT $\beta$ R<sup>-/-</sup> melanoma. Blocking the nonclassical pathway suppresses tumor growth and lymphatic metastasis by reducing chemokine production, restricting Treg recruitment to tumors, and retaining intratumoral IFN $\gamma$ <sup>+</sup> CD8 T cells. Our data reveals that Treg LT $\alpha$ 1 $\beta$ 2 promotes LT $\beta$ R nonclassical NF $\kappa$ B signaling in tumor cells and LECs providing a rational strategy to prevent Treg promoted tumor growth and metastasis.

Lymphotoxin (LT) beta receptor (LT $\beta$ R) is a member of the tumor necrosis factor receptor (TNFR) family and mediates unique immune functions critical for the development and maintenance of various lymphoid microenvironments, including stromal cell specialization, positioning of lymphocytes within lymph nodes (LNs), specialization of high endothelial venules, and formation of secondary lymphatic

organs and tertiary lymphoid structure organs<sup>1</sup>. LT $\beta$ R has two known ligands: the membrane-bound lymphotoxin heterotrimer (LT $\alpha$ 1 $\beta$ 2), and LIGHT (TNFSF14)<sup>2</sup>. Unlike TNFR1 that exclusively signals through the classical nuclear factor- $\kappa$ B (NF $\kappa$ B) pathway, LT $\beta$ R signals through a dual cascade that activates both classical and nonclassical NF $\kappa$ B pathways in the lymphatic endothelium<sup>2</sup>. The classical pathway acts

<sup>1</sup>Department of Surgery, University of Maryland School of Medicine, Baltimore, MD 21201, USA. <sup>2</sup>Center for Vascular and Inflammatory Diseases, University of Maryland School of Medicine, Baltimore, MD 21201, USA. <sup>3</sup>Fischell Department of Bioengineering, University of Maryland, 8278 Paint Branch Drive, College Park, MD 20742, USA. <sup>4</sup>Department of Pediatrics, Division of Blood & Marrow Transplantation & Cellular Therapy, University of Minnesota, Minneapolis, MN 55455, USA. <sup>5</sup>Institute for Pathology, Hannover Medical School, 30625 Hannover, Germany. <sup>6</sup>Department of Hematology and Oncology, Hannover Medical School, 30625 Hannover, Germany. <sup>7</sup>Institute for Genome Sciences, University of Maryland School of Medicine, Baltimore, MD 21201, USA. <sup>8</sup>Transplantation Research Center, Brigham and Women's Hospital, Harvard Medical School, Boston, MA 02115, USA. <sup>9</sup>Department of Microbiology and Immunology, University of Maryland School of Medicine, Baltimore, MD 21201, USA. <sup>10</sup>These authors contributed equally: Wenji Piao, Long Wu, Yanbao Xiong, Gregory C. Zapas.

 e-mail: [wpiao@som.umaryland.edu](mailto:wpiao@som.umaryland.edu); [jbromberg@som.umaryland.edu](mailto:jbromberg@som.umaryland.edu)

rapidly, phosphorylating the inhibitor of the kappa-B kinase (IKK) complex and degrading the inhibitor I $\kappa$ B $\alpha$ , thereby allowing for the release of the RelA/p50 complex and nuclear translocation. The non-classical pathway has a more sustained response involving the NF $\kappa$ B inducing kinase (NIK) dependent processing of p100 to p52, which dimerizes with RelB for nuclear translocation<sup>3</sup>.

While the LT system has a defined role in several important aspects of immune regulation and interactions of leukocytes and blood vascular and lymphatic endothelium, there is conflicting evidence for the role LT $\beta$ R plays in cancer cell biology. Some reports describe links of LT $\beta$ R to primary tumorigenesis related to mechanisms controlling cell survival, cell-cycle progression, and initiation of angiogenesis<sup>4</sup>. In multiple myeloma, mutations resulting in constitutive activation of the NIK pathway are frequently observed along with associated overexpression of LT $\beta$ R<sup>5</sup>. LT $\beta$ R expressing fibrosarcoma cells have been shown to interact with LT $\alpha$ 1 $\beta$ 2 expressing lymphocytes, resulting in the activation of a proangiogenic pathway required for solid tumor neovascularization<sup>6</sup>. In contrast, other reports demonstrated LT $\beta$ R activation by LIGHT promoted anti-tumor immunity<sup>7</sup>. Agonist anti-LT $\beta$ R monoclonal antibody (mAb) treatment inhibited tumor growth in colorectal cancers<sup>8</sup> and enhanced chemotherapeutic responses<sup>1</sup>. Thus, LT $\beta$ R signaling has a more complex role in the tumor microenvironment (TME) that warrants further investigation.

High frequencies of immunosuppressive regulatory T cells (Tregs) are present in the TME of various primary tumors, and these intratumoral Tregs are key suppressors of anti-tumor immunity<sup>9,10</sup>. Selectively targeting Tregs in the TME has emerged as an effective anti-tumor strategy. In our previous studies, we found that among T cell subsets, both human and mouse Tregs express the highest level of membrane-anchored LT $\alpha$ 1 $\beta$ 2, suggesting that Tregs are the predominant population to interact with LT $\beta$ R, which is highly expressed on human and mouse lymphatic endothelial cells (LECs)<sup>11,12</sup>. LT $\alpha$  deficiency prevents Treg lymphatic migration to draining LNs and impairs their suppressive function in models of allograft protection<sup>11</sup>. Engagement of LT $\beta$ R on LECs by LT $\alpha$ 1 $\beta$ 2<sup>+</sup> but not LT $\alpha$ <sup>-/-</sup> Tregs induces LEC basal protrusions that support Treg afferent transendothelial migration (TEM)<sup>11</sup>. Blood endothelial cells, including high endothelial venules (HEV) also express high levels of LT $\beta$ R. However, the LT $\alpha$ 1 $\beta$ 2-LT $\beta$ R interaction is not required for Treg cell migration from blood through HEV into the LNs<sup>11</sup>, although deletion of endothelial LT $\beta$ R in mice impairs LN homing of conventional T cells and B cells through impaired integrin and selectin expression by HEV<sup>13</sup>. Since tumor cells also express LT $\beta$ R, Tregs may also have a direct impact on tumor cells through LT $\alpha$ 1 $\beta$ 2/LT $\beta$ R pathways.

While LT $\alpha$ 1 $\beta$ 2-LT $\beta$ R interaction is integral to many aspects of immune cell migration and endothelial cell responses, there are limited studies that address the roles that LT $\beta$ R may play in cancer cell migration, interactions with blood or lymphatic endothelium, and initiation of metastasis. Previous studies<sup>1,8,14</sup> assessing the role of LT $\beta$ R in cancer have used approaches that relied on total receptor blockade or activation with pharmacologic or genetic interventions but did not dissect the contributions of each bifurcated LT $\beta$ R signaling cascade to specific cell processes, including migration patterns. A more in-depth understanding can be obtained only with selective targeting of the LT $\beta$ R-mediated classical or nonclassical NF $\kappa$ B signaling pathway. In our previous studies, we constructed and validated cell permeable decoy receptor peptides based on the LT $\beta$ R cytoplasmic TRAF recruitment domains<sup>3</sup>. These peptides were capable of selectively and specifically targeting each arm of the LT $\beta$ R-NF $\kappa$ B signaling pathways.

Since most solid tumors contain both tumor and stroma cells, including LECs which form lymphatic vessels for transporting metastatic and immune cells to draining LNs, we focused on LT $\beta$ R signaling in tumor cells and LECs. We used these LT $\beta$ R decoy peptides to selectively target either classical or nonclassical NF $\kappa$ B signaling

pathway in melanoma cells and LECs to dissect the molecular underpinnings related to cancer cell migration and metastasis in vitro and in vivo syngeneic mouse melanoma model whose metastasis follow reliable lymphatic routes<sup>15</sup>. In this work, we demonstrate that selective inhibition of tumor and LEC LT $\beta$ R nonclassical NF $\kappa$ B signaling pathway suppresses human and mouse melanoma and other cancer cell growth and TEM in vitro. When applied to an in vivo mouse model of melanoma metastases, the LT $\beta$ R nonclassical NF $\kappa$ B blocking peptide limits tumor cell and immune cell lymphatic migration into the tumor-draining LNs and induces tumor regression. Mechanistically, constitutively activated tumor LT $\beta$ R nonclassical NF $\kappa$ B signaling harnesses chemokines and interferon-regulated genes, which promotes immune suppressive cell recruitment, especially Tregs which further enhance LT $\beta$ R nonclassical NF $\kappa$ B signaling in tumor cells and LECs. These results indicate a general reliance on LT $\beta$ R signaling in cancer cell migration and the initiation of lymphatic-based metastases that could be utilized for novel therapeutic modalities.

## Results

### High LT $\beta$ R expression on tumors denotes a worse patient prognosis

To assess LT $\beta$ R expression and its association with phenotype and clinical characteristics in human cancer samples, The Cancer Genome Atlas (TCGA) gene expression data and the Human Protein Atlas were queried for LT $\beta$ R expression levels and patient survival. High LT $\beta$ R expression on tumors was associated with poor survival in patients with breast cancer, head and neck cancer, lung cancer, renal cancer, and cutaneous melanoma (Fig. 1a). LT $\beta$ R expression levels were comparable with many oncogenes such as MYC, TP53, and BRCA1 in melanoma patients (Fig. 1b), supporting that high LT $\beta$ R expression on tumors denotes worse patient prognosis. Cancer patient samples were stratified as high and low LT $\beta$ R expressors using an expression cut-off of one standard deviation above and below the mean of normalized gene expression. The clustering of gene expression of high and low LT $\beta$ R expression cohorts of melanoma patients was assessed using principal component analysis (PCA). There was distinct clustering of samples, indicating underlying differences between LT $\beta$ R high and low expressing melanomas (Fig. 1c). To identify other genes that may play an important role alongside LT $\beta$ R, we analyzed differential gene expression (DGE) between the high and low LT $\beta$ R expression cohorts. We identified 3285, 2134, and 3285 DEGs for melanoma, breast cancer, and lung cancers, respectively, with an adjusted  $p$  value  $<0.05$  and at least a twofold change in gene expression (Fig. 1d–f). Among all three types of cancers, we identified shared DEGs that were upregulated in LT $\beta$ R high cohorts, including chemotactic chemokines (CCL20, CCL21, CXCL1, CXCL2, and CXCL5)<sup>16</sup>; Sox F genes (SOX7, SOX17, and SOX18) which play important roles on angio- and lymphangiogenesis<sup>17,18</sup>, and S100A family genes (such as S100A4 and S100A9) with well-established roles in tumor metastases and invasion<sup>19,20</sup>. Functional gene ontology (GO) enrichment for skin cutaneous melanoma revealed 272 GO terms with an adjusted  $p$  value  $<0.01$ . The top ten significantly enriched signaling activities identified in LT $\beta$ R high cohorts (Fig. 1g) were related to regulation of cellular chemotaxis, immune cell activation and migration, and regulation of inflammatory responses.

### Most tumor cells express LT $\beta$ R which signals by classical and nonclassical pathways

Several murine and human tumor cells of diverse histologic origins were assessed for LT $\beta$ R expression by flow cytometry. Most tumor cells expressed high levels of LT $\beta$ R (Supplementary Table 1), including the well-studied B16F10 murine and human A375 melanoma cell lines (Fig. 2a). Indeed, analyzing the major component cells of human melanoma or breast cancer using published single-cell RNA sequencing data, we found LT $\beta$ R is highly expressed on cancer cells and

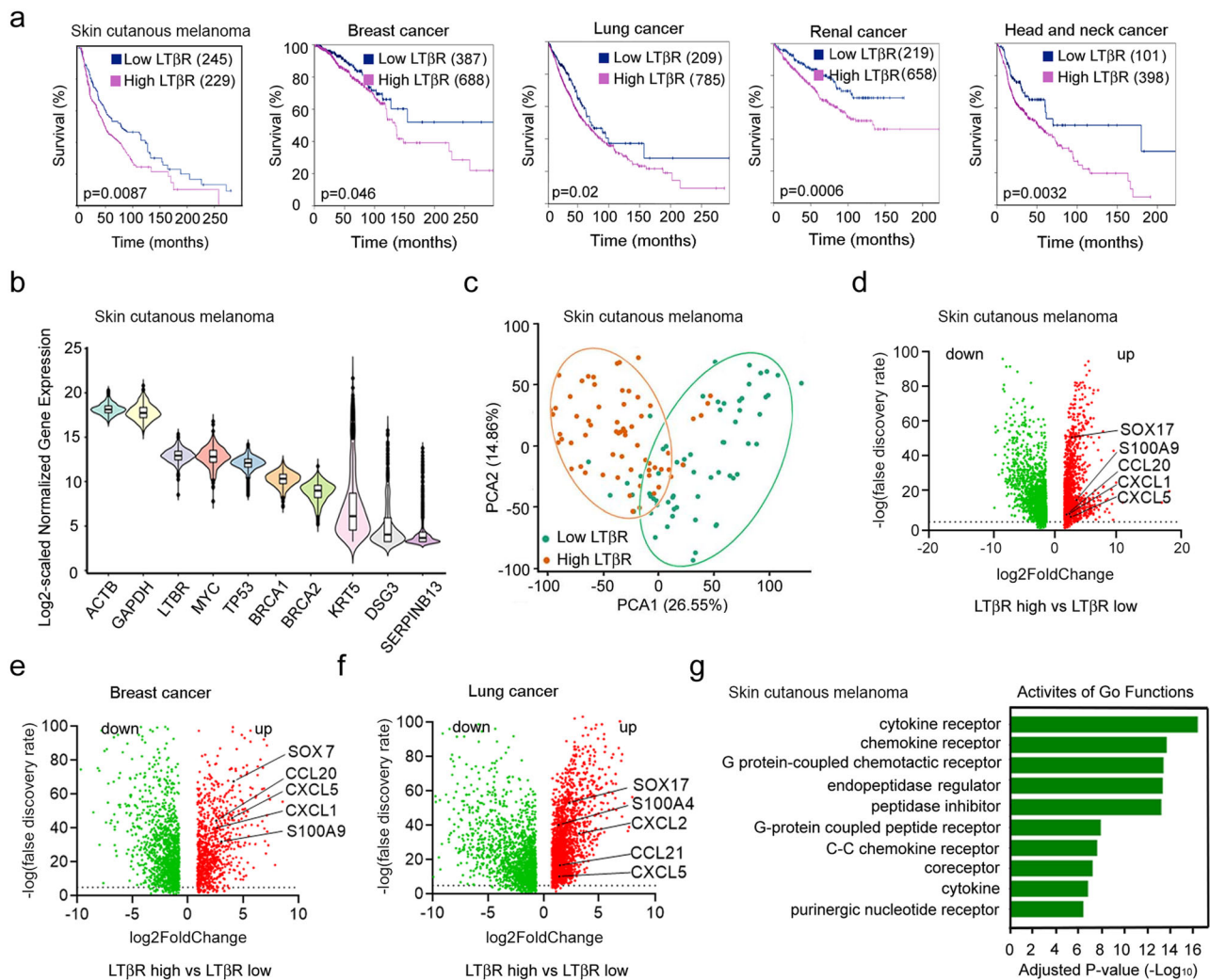


**Fig. 1 | High LT $\beta$ R expression in tumors is associated with poor survival in cancer patients.** **a** Kaplan–Meier survival analysis of LT $\beta$ R expression (derived from Human Protein Atlas and TCGA data) in various cancer cohorts. “Low” versus “high” data segregated based on one standard deviation below or above the mean expression of LT $\beta$ R, Mantel–Cox log-rank test. **b** The violin and box plots depict the differential expression of selected genes across skin cutaneous melanoma ( $n = 472$  samples) reveals that increased LT $\beta$ R gene expression is comparable with various oncogenes. The inset box bounds the interquartile range divided by the median, with the whiskers extending to a maximum of 1.5 times the interquartile range beyond the box. **c** Principal component analysis (PCA) from TCGA melanoma cohort for LT $\beta$ R “high” versus “low” LT $\beta$ R subsets ( $n = 59, 60$ , respectively).

**d–f** Volcano plot analysis evaluating differentially expressed genes (DEGs) from LT $\beta$ R “high” versus “low” LT $\beta$ R cohort of TCGA skin cutaneous melanoma patients ( $n = 35, 43$ , respectively) (**d**),  $n = 3285$ ; breast cancer patients ( $n = 96, 130$ , respectively) (**e**),  $n = 2134$ ; and lung cancer patients ( $n = 68, 39$ , respectively) (**f**),  $n = 3285$ , adjusted  $p$  value  $< 0.05$  and  $> 2$ -fold change in gene expression. **g** Gene ontology (GO) enrichment analysis in 272 GO terms for TCGA skin cutaneous melanoma. The  $p$  value reflects the association between a set of genes in the TCGA dataset and a biological function is significant (adjusted  $p$  value  $< 0.01$ ). The top ten statistically significant pathways are shown.  $P$  values are calculated using a two-tailed  $t$ -test and adjusted using Benjamini and Hochberg’s approach. Source data are provided as a Source Data file.

endothelial cells (Supplementary Fig. 1a–c). while its ligand genes LT $\alpha$  and LT $\beta$  are predominantly expressed in T cells and B cells, and Tregs have the highest combined expression levels of LT $\alpha$  and LT $\beta$  (Supplementary Fig. 1d, e).

To determine LT $\beta$ R-mediated classical and nonclassical NF $\kappa$ B signaling in tumor cells, we stimulated B16F10 cells with agonist anti-LT $\beta$ R mAbs along with pretreatment with cell-permeable LT $\beta$ R blocking decoy peptides, which we previously developed and validated to selectively block LT $\beta$ R-classical NF $\kappa$ B- $\text{IKK}\beta$ /p65 (ciLT) or nonclassical NF $\kappa$ B- $\text{IKK}\alpha$ /NIK/p52 (nciLT) pathways<sup>3</sup>. Unstimulated cells in a steady state showed weak  $\text{IKK}\alpha$ / $\beta$  and NF $\kappa$ B-p65 phosphorylation, which were not affected by either ciLT or nciLT blocking peptides (Fig. 2b, left panel). LT $\beta$ R ligation induced phosphorylation of  $\text{IKK}\alpha$ / $\beta$  (Fig. 2b, right panel), which was inhibited by both ciLT and nciLT 5 to 20 min post ligation. LT $\beta$ R ligation further enhanced NF $\kappa$ B-p65 phosphorylation, which was inhibited as early as 5 to 10 min by ciLT but not

nciLT (Fig. 2b, right panel). Resting B16F10 cells had constitutively processed p52 and was inhibited by nciLT only (Fig. 2c, left panel). Ligation of LT $\beta$ R further enhanced p52 processing which was inhibited by nciLT but not ciLT (Fig. 2c, right panel). Immunoprecipitation of LT $\beta$ R showed a low level of TRAF2 and no TRAF3 bound to the B16F10 LT $\beta$ R complex in the steady state (Fig. 2d, left panel). Stimulation of LT $\beta$ R recruited TRAF3, and this binding was blocked by nciLT alone (Fig. 2d, right panel). Notably, stimulation of LT $\beta$ R also recruited more TRAF2 to the receptor complex, which was blocked by both ciLT and nciLT (Fig. 2d, right panel). These data suggest that B16F10 LT $\beta$ R nonclassical NF $\kappa$ B signaling involves the recruitment of both TRAF2 and TRAF3 to the LT $\beta$ R complex, while LT $\beta$ R-classical NF $\kappa$ B signaling mainly requires TRAF2 recruitment. Similar signaling patterns were observed in human melanoma A375 cells (Fig. 2e, f). Together, these data show that nciLT preferentially blocks B16F10 LT $\beta$ R nonclassical NF $\kappa$ B signaling. Interestingly, nciLT suppressed  $\text{IKK}\alpha$ / $\beta$  but not p65



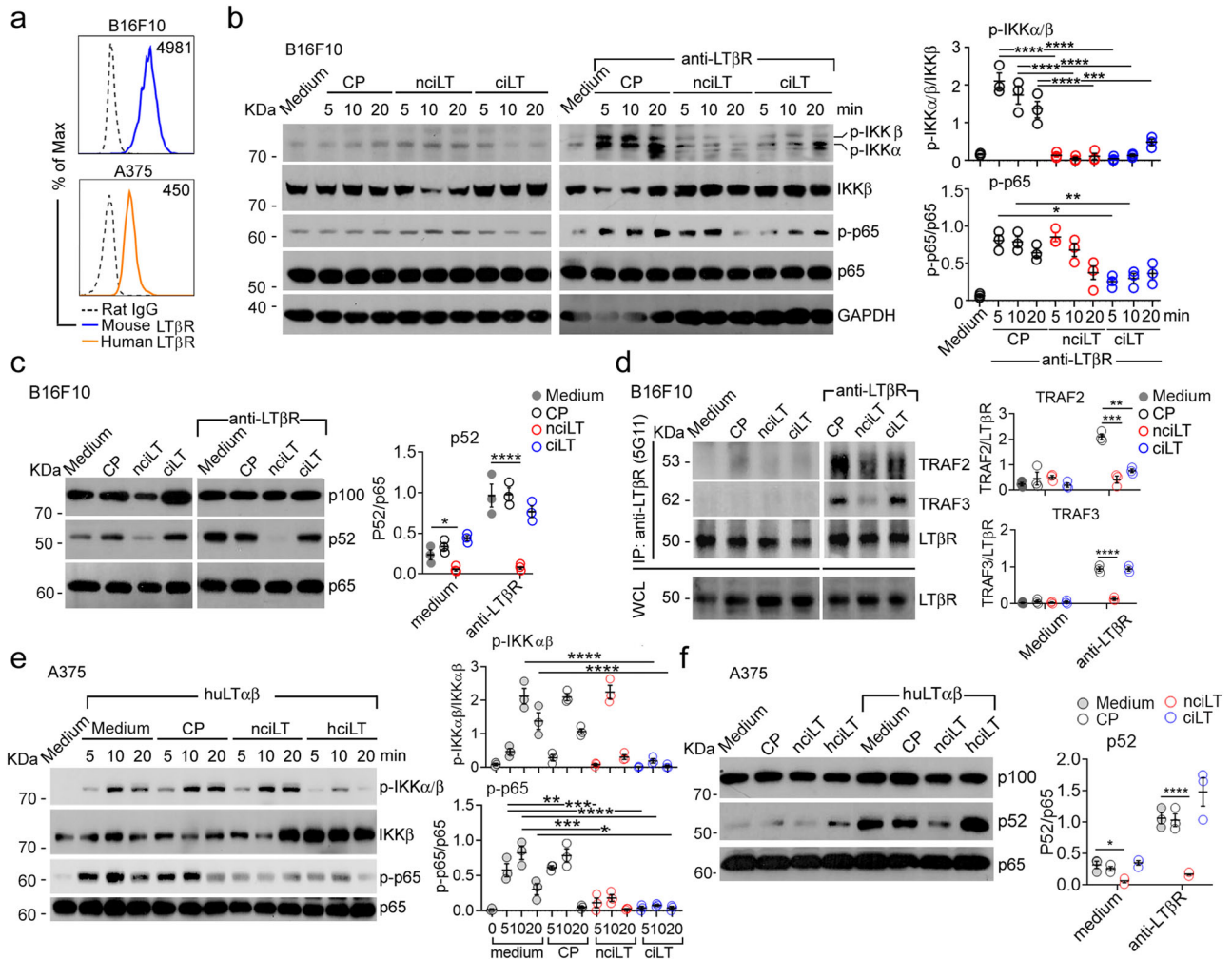


**Fig. 2 | Tumor LTβR signals by classical NFκB and nonclassical NFκB pathways.** **a** Flow cytometry of LTβR expression on mouse (B16F10) and human (A375) melanoma cells. Median fluorescence intensity (MFI) shown. **b, c** Immunoblots for classical IKKα/β (p-IKKα/β) (\*\*\**P* = 0.0005) and NFκB-p65 phosphorylation (p-p65) (\**P* = 0.0109, \*\**P* = 0.0021) (**b**), and nonclassical p100 processing to p52 (\**P* = 0.0459) (**c**) in B16F10 pretreated with 20 μM ciLT, nciLT, or control scrambled peptide (CP) for 1 h at 37 °C; and then stimulated with or without agonist anti-LTβR 3C8 mAb (2 μg/mL) for indicated times (**b**) or 6 h (**c**). Representative blots shown, quantification of phospho-p65 or p52 and IKKα/β are normalized to p65 and IKKα/β respectively. **d** Immune precipitation of B16F10 LTβR with anti-LTβR mAb (5G11). Cells stimulated with or without agonist anti-LTβR mAb for 10 min. Representative

blots are shown. Quantification of the bound TRAF2 (\*\**P* = 0.0004, \*\*\**P* = 0.0001) or TRAF3 (\*\**P* = 0.0004, \*\*\**P* = 0.0001) is normalized to the loaded LTβR expression. WCL whole cell lysate. **e, f** Human melanoma A375 cells pretreated with 20 μM human ciLT (hciLT), nciLT, or CP for 1 h at 37 °C; and then stimulated with or without 100 ng/mL human recombinant LTαβ for indicated times (**e**) or 6 h (**f**). Immunoblots for p-IKKα/β, p-p65 (nciLT: \*\**P* = 0.0019; \*\*\**P* = 0.0001; ciLT: \**P* = 0.0407, \*\*\**P* = 0.0002), and p52 (\**P* = 0.0242). Each panel is representative of three independent experiments. **b–f** Mean ± SEM. *P* values are calculated by two-way ANOVA, Sidak’s multiple comparisons test. \*\*\*\**P* < 0.0001. Uncropped gels and Source data are provided as a Source Data file.

phosphorylation in mouse melanoma and suppressed p65 but not IKKα/β phosphorylation in human melanoma, indicating cellular context-dependent classical NFκB signaling. It is noteworthy that the same peptide blocks TRAF recruitment to LTβR differently in tumor cells and LECs: nciLT blocks both TRAF2 and TRAF3 binding in B16F10 but blocks only TRAF3 in LECs<sup>3</sup>, while ciLT blocks only TRAF2 in B16F10 but blocks both TRAF2 and TRAF3 in LECs<sup>3</sup>, again indicating cellular context-dependent LTβR signaling.

**Tumor LTβR nonclassical NFκB signaling preferentially regulates TEM**

We previously characterized the role of LTβR in migration and its regulation by Tregs, endothelial cells<sup>3,11,12</sup>. Focusing on melanoma and breast cancer, which follow reliable routes of lymphatic metastasis<sup>15</sup>, we used the specific blocking peptides to investigate which LTβR signaling pathways regulate tumor lymphatic TEM. We treated mouse and human tumor cell lines with the decoy peptides or with the agonist

anti-LTβR mAb and assessed their migration across Boyden chamber transwells coated with the mouse lymphatic endothelial cell line SVEC4–10 or human primary LECs. To enhance migration, we used the chemotactic molecule sphingosine 1-phosphate (S1P), which is spatially compartmentalized in blood, lymph, and tumor, and has widely expressed receptors (S1P1–5)<sup>21</sup>, recapitulating migration from tissue to lymphatic vessels as would occur during metastatic spread<sup>22</sup>. The nonclassical LTβR-NFκB blocking peptide nciLT (identical sequence in human and mouse) but not classical LTβR-NFκB blocking peptide ciLT (versions specific for mouse and human used) was sufficient to inhibit TEM of murine tumor cells such as sarcoma KPI30, breast cancer 410, ovarian cancer ID8, mammary adenocarcinoma 66.1 (Fig. 3a), human breast cancer MDA-MB-231, and human melanoma A375 (Fig. 3b and Supplementary Table 2). Both nciLT and ciLT inhibited TEM of mouse melanoma B16F10 and human lung cancer A549, although nciLT was far more effective. LTβR stimulation by anti-LTβR mAb enhanced TEM of the mouse or human melanoma and breast cancer (Fig. 3a, b).

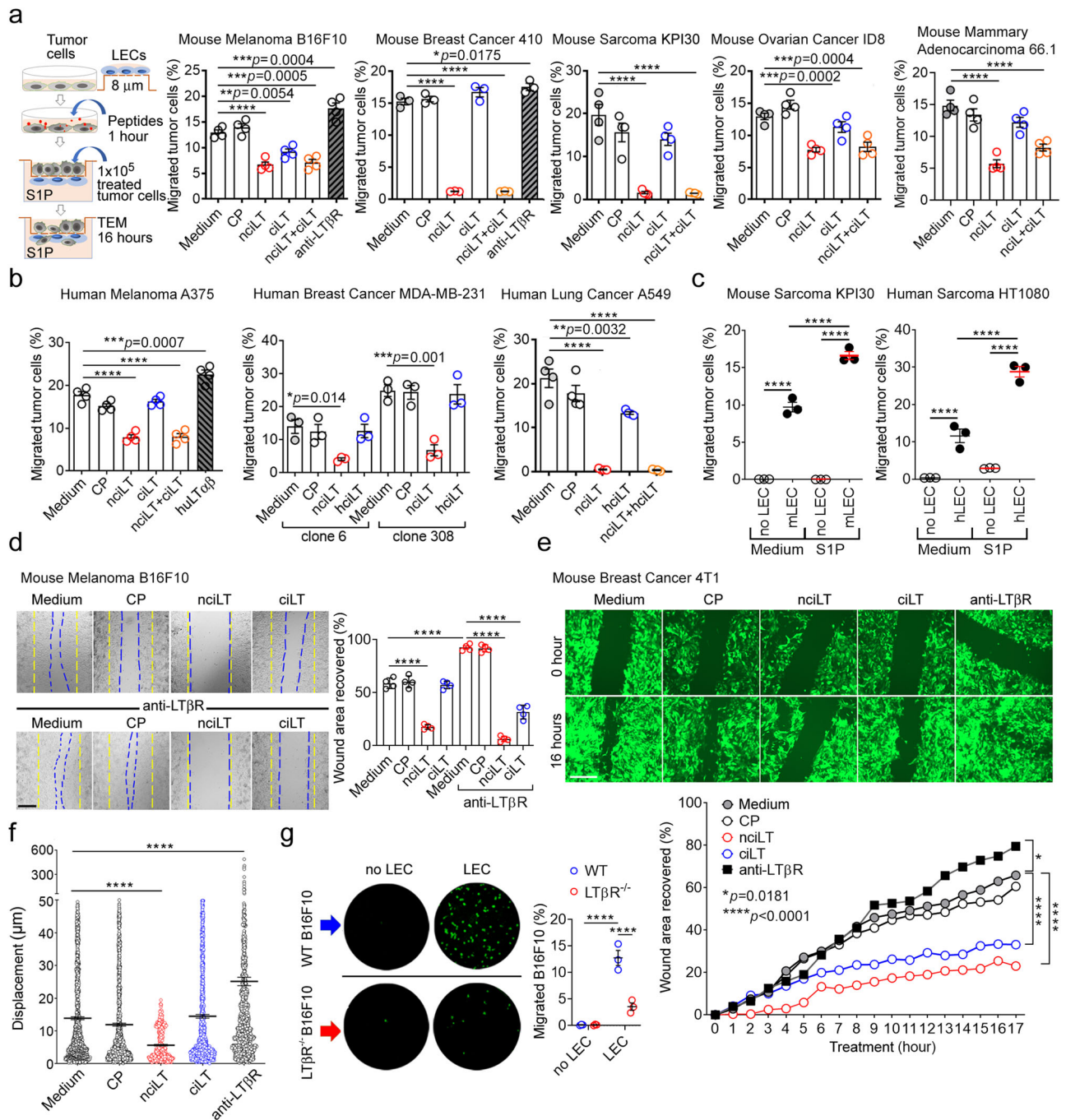


**Fig. 3 | Most tumors use nonclassical NF $\kappa$ B signaling for lymphatic migration.**

**a** Transwell assay of mouse cancer cell lines. Mouse melanoma B16F10 ( $n = 4$ ), mouse breast cancer 410 ( $n = 3$ ), mouse sarcoma KPI30 ( $n = 4$ ), mouse ovarian cancer ID8 ( $n = 4$ ), and mouse mammary adenocarcinoma 66.1 ( $n = 4$ ) cells pretreated with 20  $\mu$ M each of nciLT, ciLT, nciLT combined with ciLT, or CP for 1 h at 37  $^{\circ}$ C; or treated with 2  $\mu$ g/mL agonist anti-mouse LT $\beta$ R Ab (3C8) for 1 h at 37  $^{\circ}$ C, washed and loaded for TEM across mouse LECs toward 200  $\mu$ m SIP for 16 h.

**b** Transwell assay of human cancer cell lines. Human melanoma A375 ( $n = 4$ ), human breast cancer MDA-MB-231 ( $n = 3$ ), human lung cancer A549 ( $n = 4$ ) cells pretreated with 20  $\mu$ M each of nciLT, hciLT, nciLT combined with hciLT, or CP for 1 h at 37  $^{\circ}$ C; or treated with 100 ng/mL human LT $\beta$ R ligand huLT $\alpha$  $\beta$  for 1 h at 37  $^{\circ}$ C, washed and loaded for TEM across human LECs toward 200  $\mu$ m SIP for 16 h. **c** Transwell TEM assay of mouse or human sarcoma cells toward medium or 200  $\mu$ m SIP crossing the 8  $\mu$ m Boyden chamber coated with or without mouse or human LECs, respectively.

**d** Representative images ( $n = 4$ ) of cell migration into the area of the defect after scratching confluent B16F10 monolayers treated with indicated blocking peptides. Migration into the area of cell defect was measured after 16 h. Magnification 10 $\times$ ; scale bar 450  $\mu$ m. **e** Representative images ( $n = 4$ ) of mouse breast cancer 4T1-eGFP migration into the area of cell defect at 0 and 16 h after treatment with indicated peptides. Area recovery was measured with time-lapse microscopy. Each peptide-treated group was compared to the nontreated using a paired two-tailed  $t$ -test,  $*p = 0.0181$ ,  $****p < 0.0001$ . Magnification 10 $\times$ ; scale bar 220  $\mu$ m. **f** Time-lapse microscopy of WT B16F10-GFP pretreated with peptides as in (a–c). Samples run in triplicates. **g** TEM of WT or LT $\beta$ R<sup>-/-</sup> B16F10 across transwell coated with or without mouse LECs toward 200  $\mu$ m SIP for 16 h. One representative of three images was taken. 20 $\times$  magnification. Representative of 2 (e–g) or 3 (a–d) independent experiments. Mean  $\pm$  SEM.  $****p < 0.0001$  by one-way ANOVA. Source data are provided as a Source Data file.

Notably, tumor cell TEM required the presence of LECs for migration to an SIP gradient (Fig. 3c). This is reminiscent of our previous report that T lymphocyte chemotaxis to SIP also requires the presence of LEC for efficient migration<sup>22</sup>. This suggests that factors produced by LECs, such as adhesion or junctional molecules or chemokines, are critical for tumor migration.

### Tumor LTβR nonclassical NFκB signaling regulates cell migration and motility

Tumor cells were pretreated for 1 h with LTβR signaling blocking peptides and assessed in a migration response assay. Consistently, blockade of B16F10 or 4T1 LTβR nonclassical NFκB signaling with nciLT abolished the migration response (Fig. 3d, e). ciLT inhibited the migration response with lesser efficiency.

Monitoring peptide-treated B16F10-eGFP migration across LECs by time-lapse microscopy, we observed that nciLT suppressed tumor cell motility assessed by cell displacement while agonist anti-LTβR mAb stimulated B16F10 motility (Fig. 3f). In addition, CRISPR/Cas9 LTβR-depleted B16F10 had impaired TEM across LECs (Fig. 3g). Overall, the data demonstrates that tumor LTβR nonclassical and to a lesser extent classical NFκB signaling plays critical roles in tumor motility and migration.

### Tumor LTβR nonclassical signaling regulates tumor growth

Since LTβR expression was associated with worse prognosis and increased expression of detrimental GO terms for tumor patients, we assessed LTβR regulation of tumor growth in vitro. Pretreatment of wild-type (WT) B16F10 for 1 h with nciLT inhibited cell growth, and inhibition was abolished in CRISPR/Cas9 LTβR-depleted B16F10 (Fig. 4a), indicating that inhibition is LTβR signaling specific. Peptide treatment for 1 h with or without LTβR stimulation by agonist mAb did not affect B16F10 cell viability (Fig. 4b). However, 5 to 16 h of nciLT treatment increased B16F10 apoptosis (Fig. 4c), while other peptides with or without LTβR stimulation did not affect viability. Importantly, LTβR stimulation prevented the increased apoptosis by nciLT (Fig. 4c), indicating LTβR stimulation induced classical NFκB signaling, promoted tumor cell survival, and compensated for nciLT-triggered apoptosis. These data indicate that nciLT inhibits tumor cell growth and promotes apoptosis.

### Tumor LTβR depletion suppresses tumor growth and metastasis

CRISPR/Cas9 LTβR-depleted B16F10 cells were assessed for tumor growth and migration. Subcutaneously inoculated LTβR-depleted B16F10 cells had slower in vivo growth than WT B16F10 (Fig. 4d, e) and reduced lymphatic metastasis into the draining LNs (dLNs) (Fig. 4f). LTβR-depleted B16F10 melanoma had impaired production of tumor cell-derived CXCL1 and CXCL10 (Fig. 4g), and reduced intratumoral Tregs and myeloid-derived suppressor cells (MDSCs) but increased CD4 T cells, B cells, and unaltered CD8 T cells 13 days after melanoma inoculation, compared to WT B16F10 (Fig. 4h). Since these cells were not decreased in tumor dLNs, this suggests that LTβR depletion in tumor cells had no impact on immune cell egress from the tumor. However, the reduced Tregs and MDSCs may result from the reduced CXCL1 and CXCL10, which may recruit these CXCR2 and CXCR3 expressing cells to tumors from the blood circulation (Fig. 4h).

We explored the genes affected by LTβR depletion by whole transcriptome RNA sequencing (RNA-seq) analysis, comparing CRISPR/Cas9 LTβR<sup>-/-</sup> to WT B16F10. DEGs were observed between the two cell lines with 323 upregulated and 859 downregulated in LTβR<sup>-/-</sup> B16F10 (Fig. 4i). The enhanced expression of tumor suppressor genes such as integral membrane protein 2A (*ITM2a*) and nuclear receptor 4A3 (*NR4a3*) in LTβR-depleted B16F10 cells may contribute to cell growth inhibition, while the decreased gap junction protein alpha 1 (*GJA1*), podoplanin (*PDPN*), *NOTCH3*, and basal cell adhesion molecule 1 (*BCAMI*) which regulate cell adhesion may contribute to reduced

Treg tumor recruitment and melanoma metastasis. In addition, GO analysis indicated predominant downregulation of cell surface G-protein-coupled receptor (GPCR) signaling pathways that regulate chemotaxis, localization, and transmembrane transport, in addition to cellular component organization or biogenesis and developmental regulations as key changes induced by LTβR depletion (Supplementary Fig. 2a–c).

### Genes driven by tumor LTβR-NFκB signaling

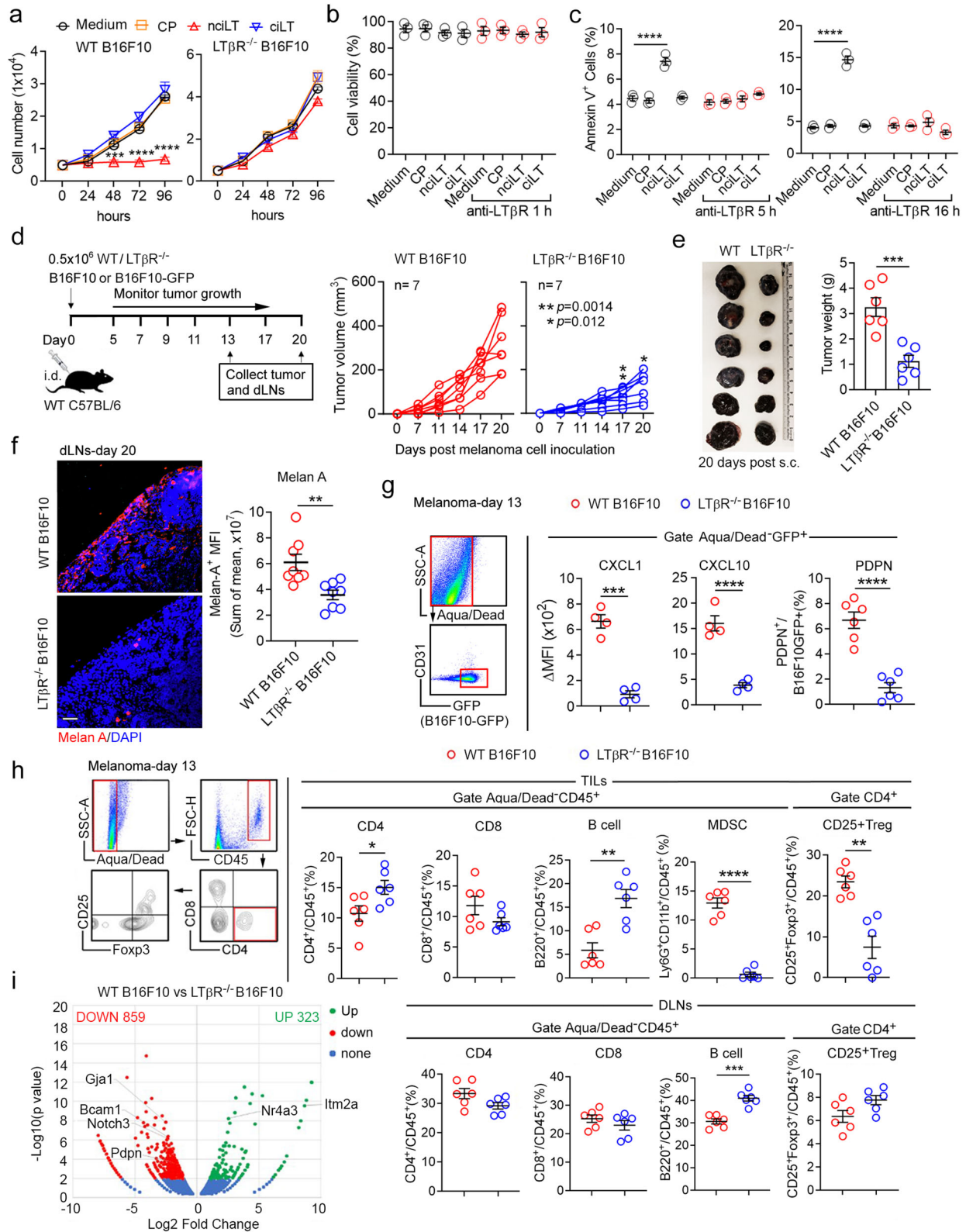
To determine the molecules regulated by nonclassical LTβR-NFκB signaling in B16F10 melanoma, we employed bulk RNASeq in a two-pronged strategy. First, we performed RNA-Seq on B16F10 cells stimulated by agonist anti-LTβR Ab (3C8) for 6 h to induce LTβR nonclassical NFκB signaling. These stimulated cells were compared to both non-stimulated B16F10 cells and to cells that were stimulated and pretreated with the LTβR-nonclassical blocking peptide nciLT. Second, we generated CRISPR/Cas9 knockout (KO) of nonclassical NFκB/NIK B16F10 and stimulated them for 6 h. Thus, we were able to compare gene expression regulated by the LTβR nonclassical NFκB pathway using both the nciLT inhibitor and NIK deficiency. Melanoma LTβR nonclassical NFκB signaling upregulated angiogenic and immunosuppressive myeloid chemokines CXCL1<sup>20,23</sup>, CXCL10<sup>24</sup>, and CCL5<sup>25</sup>, which were downregulated by nciLT and diminished in NIK-deficient B16F10 cells (Fig. 5a, b). In addition, protumor interferon-stimulated genes ISG15<sup>26</sup> and IFIT3<sup>27</sup> (interferon-induced protein with tetratricopeptide repeats 3), and oncoprotein USP18<sup>28</sup> (Ubiquitin Specific Peptidase 18), which suppresses IFN responses, were also driven by LTβR-nonclassical signaling, downregulated by nciLT, and diminished in NIK-deficient B16F10 cells (Fig. 5a). The selected genes were further confirmed by real-time PCR (Fig. 5b). CXCL1, CXCL10, and CCL5 expression were abolished in NIK-depleted but not IKKβ-depleted B16F10 (Supplementary Fig. 3a, b), confirming that these genes are regulated by the LTβR-nonclassical NFκB-NIK signaling pathway. CXCL1 and CXCL10 expression were enhanced in Treg-cocultured human melanoma A375 and human LECs and inhibited by nciLT pretreatment (Supplementary Fig. 3c, d). Neither Teff coculture nor ciLT pretreatment affected the chemokine expression. Together, the data showed that CXCL1 and CXCL10 production in tumor cells and LECs are driven by the LTβR-nonclassical NFκB-NIK signaling pathway.

A parallel strategy was employed for identifying LTβR-classical NFκB-driven genes, by comparing gene expression in cells stimulated for 1 hour with agonist mAb and pretreated or not with the classical blocking peptide ciLT, and further compared with IKKβ-depleted B16F10 (Fig. 5c). Several pro-cancer genes such as ribosomal proteins 21 and 30 (RPL21 and RPL30)<sup>29</sup>, migration and invasion enhancer 1 (MIEN1)<sup>30</sup>, and nuclear receptor NR4a1<sup>31</sup> were identified to be rapidly induced by LTβR activation and inhibited by blocking LTβR-classical NFκB signaling (Fig. 5c). Selected genes RPL21 and Mien1 were further shown by real-time PCR to be inhibited by the classical NFκB blocking peptide ciLT but not by the nonclassical NFκB blocking peptide nciLT (Fig. 5d), confirming regulation by the LTβR-classical NFκB signaling pathway.

### Treg LTα1β2 stimulates tumor LTβR nonclassical NFκB signaling to enhance tumor growth

Our previous study revealed that Tregs express high levels of LTα1β2 which ligate and activate LTβR on LEC<sup>12</sup>. Treg LTα1β2 signals primarily to the LTβR nonclassical NFκB pathway and alters LEC morphology and membrane characteristics, thereby causing endothelial morphologic changes and promoting lymphatic TEM of other immune cells<sup>12</sup>. To explore the possible role of Tregs directly interacting with tumor cells, we assessed whether Treg LTα1β2 can ligate and activate tumor surface LTβR. LTα1β2 high expressing human Tregs and LTα1β2 low expressing human effector T cells (Teffs) (Supplementary Fig. 4a) cocultured with the melanoma cells equally induced phosphorylation





of IKK $\alpha/\beta$  and p65 classical NF $\kappa$ B signaling in human A375 cells as early as 10 min after incubation (Supplementary Fig. 4b). An identical pattern was observed in mouse B16F10 cultured with mouse Tregs and Teffs (Supplementary Fig. 4c). After 5 h coculture with both human and mouse melanoma cells, only Tregs induced nonclassical NIK signaling for p100 processing to p52 in these tumor cells, while LT $\alpha$  $\beta$ -low expressing Teffs (Fig. 5e) or LT $\alpha$ -deficient Tregs (Fig. 5f) did not. Only

nonclassical blocking peptide inhibited Treg-induced nonclassical NF $\kappa$ B signaling in human melanoma (Fig. 5g), while both nciLT and ciLT inhibited the Treg-induced nonclassical signaling in B16F10 (Supplementary Fig. 4d). Other immune cells such as B cells, CD8 T cells also express LT $\alpha$ 1 $\beta$ 2, however, the expression level is significantly lower than that of Tregs (Supplementary Fig. 4e), and B cells failed to induce any NF $\kappa$ B signaling in either tumor or LECs

**Fig. 4 | Tumors use LT $\beta$ R nonclassical NF $\kappa$ B signaling for tumor growth.** **a** In vitro cell growth of WT or LT $\beta$ R<sup>-/-</sup> B16F10 pretreated with 20  $\mu$ M of CP, nciLT, or ciLT for 1 h. Cell numbers counted after 24, 48 (\*\*\* $p$  = 0.0004), 72 h (\*\*\*\* $p$  < 0.0001), 96 h (\*\*\*\* $p$  < 0.0001).  $P$  values are calculated by two-way ANOVA and Dunnett's multiple comparisons test. **b** Cell viability analysis of B16F10 treated with indicated peptide with or without anti-LT $\beta$ R mAb (3C8) for 1 h and then assessed by MTT assay. **c** Flow cytometry apoptotic cell analysis of Annexin V<sup>+</sup> B16F10 pretreated with indicated peptides for 1 h, and then stimulated with or without anti-LT $\beta$ R mAb for 5 or 16 h. \*\*\*\* $P$  < 0.0001 by two-way ANOVA. **d–h** C57BL/6 mice intradermally transferred with WT or CRISPR/Cas9 LT $\beta$ RKO (LT $\beta$ R<sup>-/-</sup>) B16F10. Scheme of experimental setup and tumor growth ( $n$  = 7). Two-way ANOVA, Sidak's multiple comparisons test. \*\* $P$  = 0.0014; \* $P$  = 0.0122. **(d)** Six representative tumors and their weights are shown **(e)**. \*\*\*\* $P$  = 0.0007 by unpaired two-tailed  $t$ -test. At day 20, Draining LNs (DLNs) were analyzed for Melan-A expression of metastatic B16F10

cells in dLNs by immunohistochemistry **(f)**. Representative images ( $n$  = 8). Magnification 20 $\times$ ; scale bar 42  $\mu$ m. \*\* $P$  = 0.0037 by unpaired two-tailed  $t$ -test. At day 13, transferred B16F10-GFP tumors analyzed for CXCL1 ( $n$  = 4, \*\*\* $p$  = 0.0002), CXCL10 ( $n$  = 4, \*\*\*\* $P$  < 0.0001), and PDPN ( $n$  = 6, \*\*\*\* $P$  < 0.0001) expression in GFP<sup>+</sup> B16F10 cells **(g)**, and also analyzed for CD4 (\* $P$  = 0.0294), CD8, Foxp3<sup>+</sup> CD4 Tregs (\*\* $P$  = 0.0025), B220<sup>+</sup> B cells (\*\* $P$  = 0.0013), CD11b<sup>+</sup> Ly6G<sup>+</sup> MDSCs (\*\*\*\* $P$  < 0.0001) in TILs ( $n$  = 6), and CD4, CD8, B cells (\*\*\* $p$  = 0.0001) and CD25<sup>+</sup> Foxp3<sup>+</sup> CD4 Tregs in dLNs ( $n$  = 6) **(h)**.  $P$  values are calculated by unpaired two-tailed  $t$ -test. The gating strategy is shown **(g, h)**. **i** Volcano plot of differential gene expression comparing LT $\beta$ R<sup>-/-</sup> to WT B16F10 ( $P$  values are justified by two-way ANOVA) by bulk RNA-Seq analysis ( $n$  = 2). Genes upregulated ( $n$  = 323, green) or downregulated ( $n$  = 859, red) at log<sub>2</sub> fold change  $\geq 2$  or  $\leq -2$  and  $P$  value < 0.05 adjusted by the Benjamin and Hochberg method. 3 **(a–c)** or 2 **(d–h)** independent experiments. **a–h** Mean  $\pm$  SEM. Source data are provided as a Source Data file.

(Supplementary Fig. 4f) and had no impact on tumor cell TEM (Supplementary Fig. 4g). These results indicate that Treg LT $\alpha$  $\beta$  exclusively induces nonclassical NF $\kappa$ B signaling on tumor cells through cell-cell interactions. To investigate the biological function of Treg-induced preferential LT $\beta$ R nonclassical NF $\kappa$ B signaling, we cocultured Tregs with B16F10, which were pretreated with or without blocking peptides to assess tumor cell growth. Treg-cocultured B16F10 demonstrated increased cell growth. Blockade of only the nonclassical NF $\kappa$ B signaling abolished Treg stimulated growth and likewise inhibited basal growth of tumor cell even without Treg pretreatment (Fig. 5h), similar to the observations in Fig. 4a. Thus, these data show that both basal constitutive and Treg-induced LT $\beta$ R-nonclassical-NF $\kappa$ B signaling in B16F10 promote tumor growth.

### Treg LT $\alpha$ 1 $\beta$ 2 stimulates tumor LT $\beta$ R nonclassical NF $\kappa$ B signaling to enhance tumor cell TEM

To determine whether Tregs directly affect tumor cell migration, we cocultured Tregs or Teffs with melanoma cells prior to migration assay across LEC-coated transwell. Treg-cocultured B16F10 cells showed enhanced TEM across LECs in a dose-dependent fashion, while Teffs induced no such effect (Fig. 5i). Human Tregs cocultured A375 also had increased TEM (Supplementary Fig. 4h). Importantly, the effect required the presence of LECs. Without LECs, the Treg-pretreated B16F10 had no enhanced TEM (Fig. 5j). Treg enhanced TEM was LT $\alpha$ 1 $\beta$ 2-LT $\beta$ R signaling dependent since LT $\alpha$ -deficient Tregs failed to increase tumor TEM (Fig. 5k). Blockade of B16F10 LT $\beta$ R nonclassical NF $\kappa$ B signaling also abolished Treg promoted tumor TEM (Fig. 5k). Similarly, Tregs but not LT $\alpha$ -deficient Tregs, enhanced 4T1 breast cancer TEM (Fig. 5l). Treg failed to increase TEM of B cell lymphoma M12.4 which has minimal levels of LT $\beta$ R expression (Fig. 5m and Supplementary Table 1). Together, these data show that Treg LT $\alpha$  $\beta$  directly ligates tumor LT $\beta$ R to activate nonclassical NF $\kappa$ B signaling and enhance tumor cell TEM. To assess in vivo Tregs direct interaction with tumor cells, we intravenously injected WT or LT $\alpha$ -deficient Tregs to LT $\beta$ R-depleted mice inoculated with WT B16F10. Thus, in this system, Treg LT $\alpha$ 1 $\beta$ 2 can only ligate and activate tumor surface LT $\beta$ R. WT Tregs significantly promoted melanoma growth, while LT $\alpha$ -deficient Tregs failed to do so (Fig. 5n). There was also increased LT $\beta$ R nonclassical signaling driven CXCL1, CXCL10, and CCL5 expression in melanoma cells in the host mice injected with WT Tregs but not with LT $\alpha$ -deficient Tregs (Fig. 5o). These results demonstrate that in vivo Treg LT $\alpha$ 1 $\beta$ 2 can directly activate tumor cell LT $\beta$ R nonclassical NF $\kappa$ B signaling.

### Treg LT $\alpha$ 1 $\beta$ 2 stimulates LEC LT $\beta$ R nonclassical NF $\kappa$ B to promote tumor growth and TEM

We previously demonstrated that Tregs stimulate LT $\beta$ R nonclassical NF $\kappa$ B signaling in LECs and thereby alter LEC characteristics for leukocyte TEM<sup>12</sup>. Since we showed above that Tregs also stimulate tumor LT $\beta$ R to alter tumor growth and TEM, we next analyzed if this signaling induced additional events between LECs and tumors. LECs were

pretreated with Tregs, the Tregs removed, and then B16F10 added to the LECs. This coculture promoted melanoma growth (Fig. 6a). Blockade of LEC LT $\beta$ R nonclassical NF $\kappa$ B with nciLT prior to coculture with Tregs abolished the activated LEC enhanced tumor cell growth (Fig. 6a, middle row). Blockade of LEC LT $\beta$ R-classical NF $\kappa$ B with blocking peptide ciLT had no effect on tumor cell growth. LECs pretreated with Teffs did not affect tumor cell growth, and the blocking peptides did not alter the lack of effect of Teffs on LEC for tumor growth (Fig. 6a, lower row). To determine whether the growth effect was from direct tumor-LEC contact or due to the secreted factors from the LECs, 0.4  $\mu$ m pore transwells were used to separate B16F10 in the upper chamber from LECs in the lower chamber. The B16F10 or the LECs were each independently cocultured with Tregs for 6 h, the Tregs were then removed, and the growth of B16F10 was assessed after another 48 h. WT or LT $\alpha$ -deficient Tregs cocultured with LECs in the lower chamber did not promote B16F10 cell growth in the upper chamber (Supplementary Fig. 5a, b), suggesting soluble cytokines/chemokines produced by activated LECs have no effect on B16F10 cell growth, and that a direct tumor-LEC cell physical contact is required for supporting tumor cell growth. To test the effect of Treg LT-triggered LEC LT $\beta$ R signaling on tumor migration, we cocultured Tregs with WT or LT $\beta$ R-deficient LEC prior to assessing tumor cell TEM. WT LECs cocultured with Tregs promoted B16F10 TEM, while LT $\beta$ R-deficient LECs cocultured with WT Tregs did not enhance B16F10 migration (Fig. 6b). WT LECs cocultured with LT $\alpha$ -deficient Tregs also had no effect on B16F10 or 4T1 TEM (Fig. 6c).

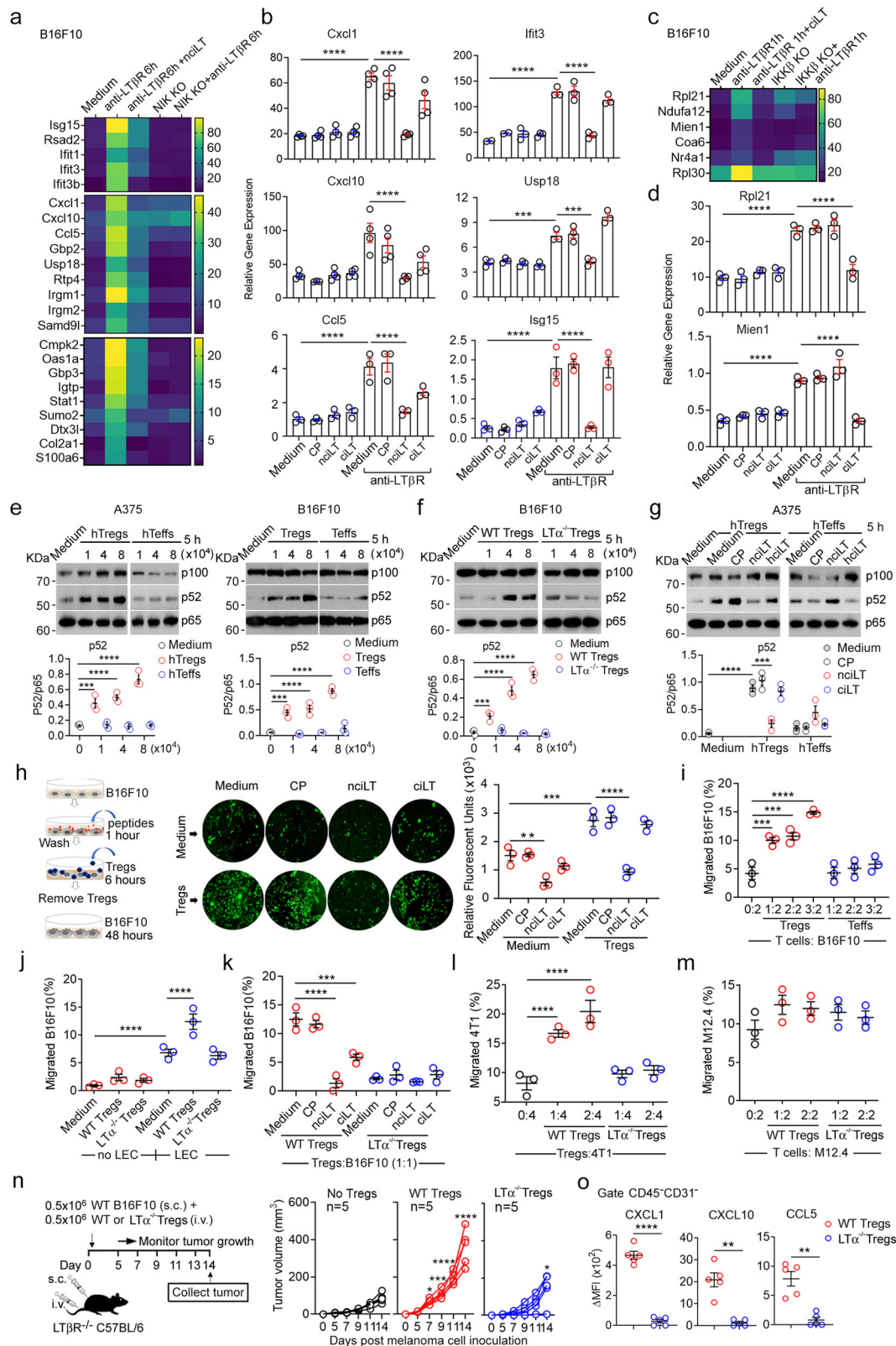
### Genes driven by LT $\beta$ R nonclassical NF $\kappa$ B signaling in LEC

To investigate which molecules are driven by LEC LT $\beta$ R signaling to regulate tumor cell growth and migration, we employed DNA microarray analysis of LECs. Primary LECs were treated with control peptide (CP), nciLT, or ciLT prior to agonist anti-LT $\beta$ R mAb stimulation. Endothelial-specific genes which promote tumor malignancy and metastasis, such as fibronectin leucine-rich transmembrane protein 2 (FLRT2), SRY-box transcription factor 18 (SOX18), and C-type lectin domain containing 14A (Clec14a), were identified to be driven by LT $\beta$ R nonclassical NF $\kappa$ B signaling and were downregulated by nciLT but not by ciLT (Fig. 6d). The selected genes were further confirmed by RT-PCR (Fig. 6e). Some genes were not transcriptionally regulated while their functions relied on post-translational changes, such as VE-cadherin which is important for endothelial integrity<sup>32</sup>. Thus, 16 h pretreatment with Tregs could transform intact zipper junctional VE-cadherin expression in lymphatic vessels (LVs) in vivo or LECs in vitro to button-like junction, while LT-deficient Tregs failed to do so (Fig. 6f).

### Treg LT $\alpha$ 1 $\beta$ 2 activates LT $\beta$ R nonclassical NF $\kappa$ B signaling on tumor-associated LECs in vivo

To study the direct in vivo influence of Treg LT $\alpha$ 1 $\beta$ 2 on LECs, we intravenously transferred  $5 \times 10^5$  WT or LT $\alpha$ <sup>-/-</sup> Tregs to WT C57BL/6





mice which were subcutaneously inoculated with  $0.5 \times 10^6$  LTBRKO B16F10. In this system, Tregs can only ligate and activate surface LTBR on stromal cells, including LECs, but not on tumor cells. Since the LTBR-deficient B16F10 had impaired tumor growth compared to WT B16F10 (Fig. 4d), WT Tregs did not significantly promote LTBR-deficient melanoma growth (Fig. 6g), although it promoted WT B16F10 (Fig. 5n). However, WT Treg but not LTα<sup>-/-</sup> Treg transfer induced more

CXCL1 and CXCL10 in the tumor LECs (Fig. 6h). WT Tregs but not LTα<sup>-/-</sup> Tregs accumulated around tumor lymphatic vessels where the nonclassical LTBR-NIK signaling driven endothelial-specific proteins FLRT2, SOX18, and Clec14 were highly upregulated (Fig. 6i and Supplementary Fig. 6a). These data indicated that in vivo Treg LTα1β2 can directly activate LTBR nonclassical NFκB signaling in tumor LECs. To study the combined in vivo influence of Treg LTα1β2 on tumor cells

**Fig. 5 | Treg LT $\alpha$ 1 $\beta$ 2 stimulates tumor LT $\beta$ R nonclassical NF $\kappa$ B pathway to promote tumor growth and TEM.** **a–d** Bulk RNA-Seq analysis of B16F10 (2 independent samples per group). Genes are downregulated by nciLT (**a**) or ciLT (**c**) and regulated by NIK (**a**) or IKK $\beta$  (**c**)-deficiency. WT or CRISPR/Cas9 NIK KO B16F10 pretreated with nciLT for 1 h followed by 6 h anti-LT $\beta$ R (3C8) stimulation (**a**, **b**). WT or CRISPR/Cas9 IKK $\beta$  KO B16F10 treated with ciLT for 1 h prior to 1 h LT $\beta$ R stimulation (**c**, **d**). Selected genes confirmed by RT-PCR for nonclassical (**b**) and classical (**d**) regulation. Relative gene expressions are normalized to HPRT gene expression. Samples are triplicated in three independent experiments. Mean  $\pm$  SEM.  $***p = 0.0001$ ,  $****p < 0.0001$  by one-way ANOVA. **e–g** Immunoblots for p100/p52 in human A357 (left panel of **e**, **g**) and mouse B16F10 (right panel of **e**, **f**) melanoma cells cocultured with various dose of human or mouse Tregs, Teffs, or LT $\alpha$ -deficient (LT $\alpha^{-/-}$ ) Tregs as indicated for 5 h. A375 pretreated with 20  $\mu$ M CP, nciLT, or hciLT for 1 h prior to coculturing with human T cells (**g**). Representative blots are shown from three independent experiments. Quantification of the protein expression of P52 normalized to p65. Uncropped gels are provided in the Source Data file. Mean  $\pm$  SEM.  $***p = 0.0002$ ,  $****p < 0.0001$  by one-way ANOVA. **h** B16F10 pretreated with 20  $\mu$ M CP, nciLT, or ciLT for 1 h, washed, and cocultured with Tregs for 6 h,

washed and grown for 48 h. One representative of three images taken from each group is shown.  $**p = 0.0036$ ,  $***p = 0.0005$  by one-way ANOVA. **i–m** Migration of B16F10 cocultured with Tregs or Teffs with various ratio (**i**). Compared to B16F10 only,  $**p = 0.0006$  (1:2),  $***p = 0.0002$  (2:2),  $****p < 0.0001$ . Migration of B16F10 cocultured with WT ( $****p < 0.0001$ ) or LT $\alpha^{-/-}$  Tregs (**j**, **k**) as indicated for 6 h, washed, and migrated across transwell coated with LECs ( $****p < 0.0001$ ) or without LEC toward 200  $\mu$ M SIP for 16 h (**j**). B16F10 pretreated with indicated peptides before coculturing with WT or LT $\alpha^{-/-}$  Tregs and TEM as in (**h**, **k**).  $***p = 0.0003$ . TEM of breast cancer 4T1 cells (**l**) or B cell lymphoma M12.4 cells (**m**) cocultured with WT or LT $\alpha^{-/-}$  Tregs with various ratios. **n**, **o**  $0.5 \times 10^6$  WT or LT $\alpha$ -deficient (LT $\alpha^{-/-}$ ) Tregs intravenously transferred to LT $\beta$ RKO (LT $\beta$ R $^{-/-}$ ) C57BL/6 mice which were subcutaneously inoculated with  $0.5 \times 10^6$  WT B16F10. Scheme of experimental setup and tumor growth (**n**).  $p$  value of tumor growth ( $n = 5$  mice) determined by two-way ANOVA Tukey's multiple comparisons test.  $*p = 0.0394$ ,  $***p = 0.0008$ ,  $****p < 0.0001$ . At day 14, tumors ( $n = 5$ ) analyzed for CXCL1 ( $****p < 0.0001$ ), CXCL10 ( $***p = 0.0002$ ), and CCL5 ( $***p = 0.0004$ ) expression. Data representative of 3 (**b**, **d**, **e–m**) and 2 (**n**, **o**) independent experiments. **b**, **d**, **e–i**: Mean  $\pm$  SEM.  $****p < 0.0001$  by one-way ANOVA. Source data are provided as a Source Data file.

and LECs for tumor growth, we intravenously transferred  $0.5 \times 10^6$  WT or LT $\alpha^{-/-}$  Tregs to WT C57BL/6 mice transplanted with  $0.5 \times 10^6$  B16F10. WT Tregs significantly promoted melanoma growth, while LT $\alpha^{-/-}$  Tregs failed to do so, suggesting the stronger impact of Treg LT $\alpha$ 1 $\beta$ 2 on tumor cells than on LECs for LT $\beta$ R-mediated tumor growth (Supplementary Fig. 6c).

To study whether in vivo LT $\beta$ R depletion affected tumor growth, we transplanted WT B16F10 into WT or LT $\beta$ RKO C57BL/6 mice, which have lymphatics but lack LNs<sup>33</sup>. Transplanted tumors in LT $\beta$ RKO mice had significantly reduced tumor growth, angiogenesis, and lymphangiogenesis compared to those in WT mice (Fig. 6j, k), and survival was also significantly higher in LT $\beta$ R-deficient mice (Fig. 6l). Analysis of TILs in LT $\beta$ RKO mice revealed reduced CD25<sup>+</sup>Foxp3<sup>+</sup>Tregs (Fig. 6m), Ly6G<sup>+</sup>CD11b<sup>+</sup>MDSCs, and F4/80<sup>+</sup>CD11b<sup>+</sup>macrophages, and increased total CD4 T cells, IFN $\gamma$ <sup>+</sup>CD8 T cells, and B220<sup>+</sup>B cells compared to those of WT mice, although total CD45<sup>+</sup> immune cells and CD8 T cells remain unchanged (Supplementary Fig. 6b). These data suggest that recipient LT $\beta$ R regulated recruitment and/or retention of Tregs, MDSCs, and macrophages into the tumor. Since LT $\beta$ R-deficient mice lack LNs, tumor lymphatic metastasis could not be directly observed<sup>33</sup>. Therefore, we then injected B16F10 i.v. to study tumor pulmonary metastasis. LT $\beta$ R-deficient mice had significantly reduced metastatic colonies in the lung compared to WT mice. Importantly, when LT $\beta$ R-deficient mice were injected i.v. with B16F10 together with WT LT $\beta$ R-sufficient primary mouse LECs, there were remarkably increased pulmonary metastases (Fig. 6n), suggesting that LT $\beta$ R on LECs plays a critical role in tumor metastases.

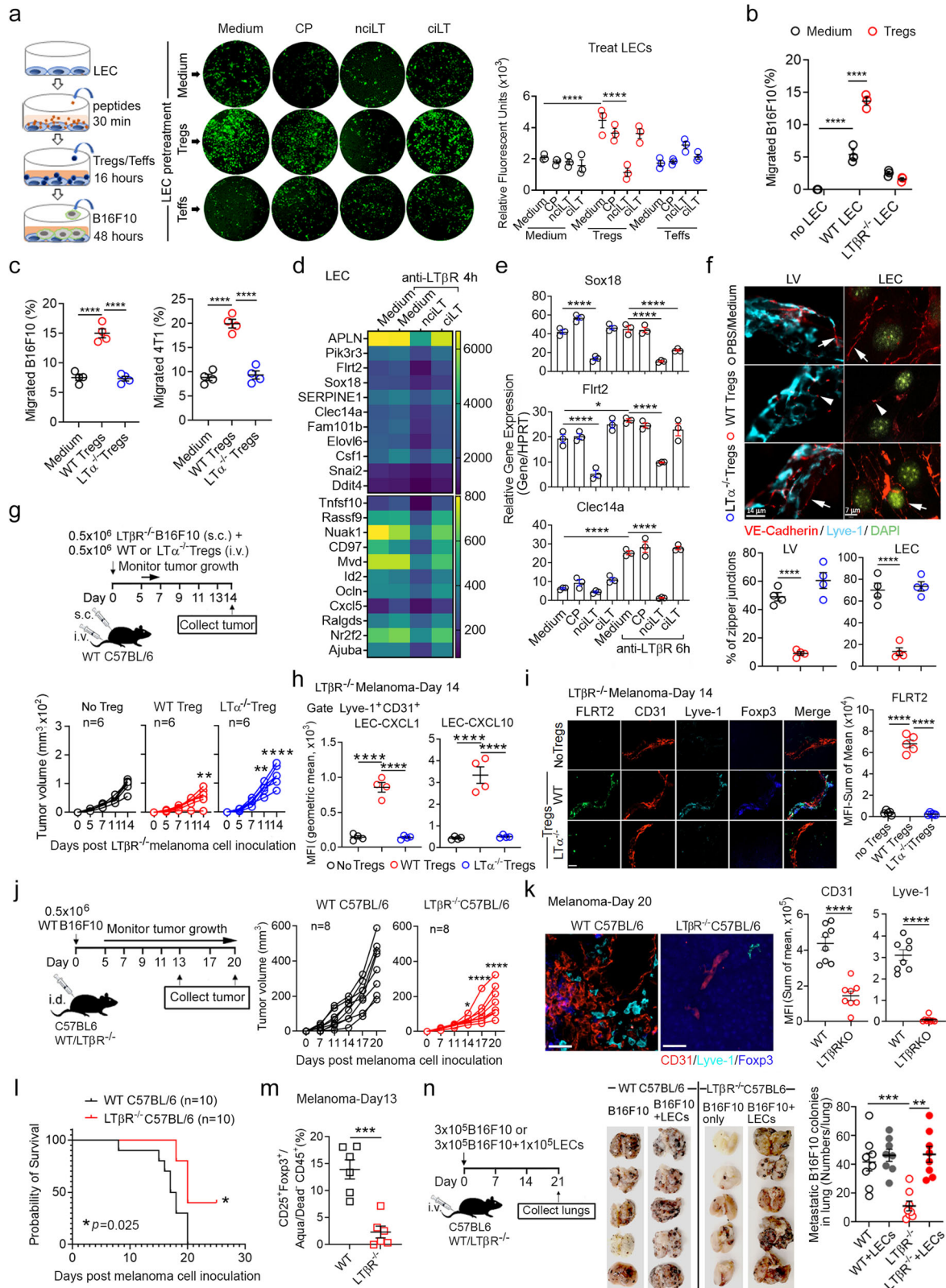
### Selective blockade of LT $\beta$ R-classical and nonclassical NF $\kappa$ B inhibits tumor growth and lymphatic metastasis

LT $\beta$ R signaling was assessed for its effects on tumor growth and metastasis by using the blocking peptides in mouse melanoma (Fig. 7a). nciLT dramatically suppressed melanoma growth, while ciLT-treated melanoma had early regression but relapsed later (Fig. 7b). nciLT or ciLT treated melanoma at day 13 after B16F10 intradermal inoculation had increased intratumoral CD4 and CD8 T cell infiltration (Fig. 7c, upper panel). In addition, both nciLT and ciLT treated tumors had increased IFN $\gamma$ -producing CD8 T cells, but no significant changes in IFN $\gamma$ <sup>+</sup> CD4 T cells (Fig. 7c, middle panel). nciLT but not ciLT significantly reduced intratumoral activated CD25<sup>+</sup> Tregs (Fig. 7c, lower panel). In contrast, ciLT increased the CD25<sup>-</sup> Treg subset. Both peptides significantly reduced granulocytic Ly6G<sup>+</sup>CD11b<sup>+</sup> MDSC and B220<sup>+</sup> B cell infiltration at day 13. Notably, only nciLT suppressed melanoma and endothelium-derived CXCL1 and CXCL10 expression (Fig. 7d). Moreover, both blocking peptides suppressed tumor angiogenesis and lymphangiogenesis by reducing CD31<sup>+</sup>lyve-1<sup>+</sup> blood vessels and

CD31<sup>+</sup>lyve-1<sup>+</sup> lymphatic vessels (Fig. 7e–g). Importantly, LT $\beta$ R-nonclassical NF $\kappa$ B-driven SOX18, a crucial transcriptional regulator of angiogenesis<sup>34</sup>, and FLRT2 which are highly expressed in LECs and facilitate tumor aggressiveness<sup>35,36</sup>, were significantly reduced in lymphatic vessels in nciLT-treated melanoma. ciLT also suppressed their expression but less effectively than nciLT (Fig. 7e–g). SOX18 localized in both blood (CD31<sup>+</sup>lyve-1<sup>+</sup>) and lymphatic vessels (CD31<sup>+</sup>lyve-1<sup>+</sup>), while FLRT2 mainly localized on lymphatic vessels alone (Figs. 7e, f, h). In dLNs, nciLT reduced both CD4 and CD8 T cells, while ciLT reduced CD4 but not CD8 T cells (Fig. 8a, upper panel), suggesting nciLT inhibited CD4 and CD8 T cell tumor egress, while ciLT inhibited CD4 T cell tumor egress which may contribute to the increased intratumoral CD4 Tregs. The total number of Tregs in dLNs were significantly decreased by both nciLT and ciLT (Fig. 8a, lower panel; 8b). Analysis of dLNs 20 days after melanoma development revealed that both nciLT and ciLT-treated mice had significantly reduced dLN melanoma metastasis and Tregs (Fig. 8b). The increased retention of IFN $\gamma$ -producing CD8 T cells in tumor-infiltrating lymphocytes (TILs) and reduced CD25<sup>+</sup>Tregs in tumor and dLNs in LT $\beta$ R blocking peptides treated melanoma may play critical roles for anti-tumor immunity.

## Discussion

Here we report that contact-dependent tumor LT $\beta$ R-NF $\kappa$ B-NIK signaling triggered by Treg LT $\alpha$ 1 $\beta$ 2 plays a critical role in tumor growth and metastases. In the TME, a high frequency of Tregs is associated with a poor prognosis in many cancers<sup>37,38</sup>. However, effective approaches to selectively targeting intratumoral Tregs are limited. Beyond the known function of immunosuppression, activated Tregs exert other multifaceted functions, such as direct dialog with endothelial cells to regulate TEM of other immune cells<sup>12,39</sup>. Our current and previous data<sup>11,12</sup> and published single-cell RNA sequencing data<sup>40,41</sup> have shown that human and mouse CD4 Tregs express the highest level of LT $\alpha$ 1 $\beta$ 2, while LT $\beta$ R is predominantly expressed on most tumor cells and endothelial cells<sup>42,43</sup>. The TCGA datasets showed high LT $\beta$ R expressing patients with cancer have a worse prognosis, suggesting anti-LT $\beta$ R as a potential therapy. However, both blockade and activation of LT $\beta$ R have shown anti-tumor efficacy<sup>1,6</sup>. Activation of LT $\beta$ R with agonist mAb has been shown to induce both tumor apoptosis and promotion<sup>1,6,44</sup>. The seemingly conflicting observations might be due to the bifurcation of LT $\beta$ R-NF $\kappa$ B signaling. We confirmed that LT $\beta$ R on the mouse and human melanoma and breast cancer cells signal through classical NF $\kappa$ B-IKK $\beta$ -p65 and nonclassical NF $\kappa$ B-NIK-p52. Dissimilar to primary LEC LT $\beta$ R, which constitutively binds TRAF3 and recruits TRAF2 upon activation, B16F10 LT $\beta$ R constitutively binds TRAF2 and recruits TRAF3 for activation. nciLT blocked both TRAF2 and TRAF3 binding to the B16F10 LT $\beta$ R complex, while blocking only TRAF3 binding to LEC



LTβR<sup>3</sup>. Thus, nciLT not only inhibited melanoma LTβR-nonclassical NFκB-NIK-p52 but also inhibited B16F10 LTβR-classical NFκB-IKKβ-p65 signaling.

LTβR-nonclassical NFκB-NIK signaling has been implicated to upregulate metastatic genes and promote cancer cell lymphatic migration in head and neck cancer which has high levels of NIK and RelB expression<sup>45</sup>, however, selective targeting of the LTβR-

nonclassical NFκB-NIK pathway has not been studied. Here we employed specific LTβR receptor decoy permeable peptides to examine tumor TEM. LTβR nonclassical NFκB blocking peptide nciLT but not classical blocking peptide ciLT inhibited TEM of most tumors, including human melanoma and mouse and human breast cancer. B16F10, 4T1, and A549 TEM or migration responses were also inhibited by ciLT but with lesser efficacy, and these cell type-dependent effects



**Fig. 6 | Tregs communicate with LEC through LT $\alpha$ 1 $\beta$ 2/LT $\beta$ R signaling to activate nonclassical NF $\kappa$ B pathway and promote tumor growth and TEM.**

**a** Peptide-pretreated LEC cocultured with Tregs or Teffs (LEC: T cell = 1: 2) for 16 h, followed by removal of T cells, and then LEC cocultured with B16F10-GFPs (LEC: B16F10 = 1:1) for 48 h. Representative images of B16F10-GFPs in triplicated wells analyzed by EVOS microscopy. **b, c** Transwell assay, B16F10-GFPs migrated across WT or LT $\beta$ R<sup>-/-</sup> LECs pretreated with or without Tregs as in **(a, b)**. B16F10 or 4T1 cells migrated across LECs pretreated with WT or LT $\alpha$ <sup>-/-</sup>Tregs for 16 h **(c)**. **d** Heatmap of gene array analysis of mouse primary dermal LECs treated with nciLT and ciLT. LECs were treated with 20  $\mu$ M nciLT or ciLT for 30 min prior to LT $\beta$ R stimulation with anti-LT $\beta$ R Ab (3C8) for 4 h. Three independent samples per group. **e** Regulated genes selected for real-time PCRs. Mouse LECs pretreated with 20  $\mu$ M indicated peptides for 30 min, washed and treated with or without anti-LT $\beta$ R Ab (3C8) for 6 h. Triplicated samples were measured in three independent experiments. \* $p$  = 0.03, \*\*\*\* $p$  < 0.0001 by one-way ANOVA. **f** Immunohistochemistry of intercellular VE-cadherin in lymphatic vessels (LV) or cultured LECs pretreated with WT or LT $\alpha$ <sup>-/-</sup>Tregs for 16 h. One representative of four images of each group. Magnification 60x; scale bar:14  $\mu$ m (LV) and 7  $\mu$ m (LEC). **g–i** Intravenous transfer of WT or LT $\alpha$ <sup>-/-</sup>Tregs ( $5 \times 10^5$ ) to WT C57BL/6 mice subcutaneously inoculated with LT $\beta$ RKO

B16F10 ( $5 \times 10^5$ ). Scheme of experimental setup and tumor growth **(g)**.  $p$  value of tumor growth ( $n = 6$ ) determined by two-way ANOVA Tukey's multiple comparisons test. \*\* $p$  = 0.0017, \*\*\*\* $p$  < 0.0001. At day 14, tumors ( $n = 4$ ) were analyzed for CXCL1 and CXCL10 expression in LECs by flow cytometry analysis **(h)**; One representative of 6 images of FLRT2 expression in tumor LECs by Immunohistochemistry **(i)**. Magnification 20x; scale bar:42  $\mu$ m. **j–m** Intradermal transfer of B16F10 cells ( $5 \times 10^5$ ) to WT or LT $\beta$ R<sup>-/-</sup> C57BL6 mice.  $p$  value of tumor growth ( $n = 8$ ) calculated by two-way ANOVA, Sidak's multiple comparisons test, \* $p$  = 0.0362, \*\*\*\* $p$  < 0.0001 **(j)**. One representative of eight images of tumor (day 20) blood (CD31<sup>+</sup>Lyve-1<sup>-</sup>) and lymphatic (Lyve-1<sup>+</sup>) vessels by immunohistochemistry (magnification 20x; scale bar 40  $\mu$ m) **(k)**, mouse survival (10 mice each group) **(l)**  $p$  value is calculated by log-rank (Mantel–Cox) test, \* $p$  = 0.025. and intratumoral Foxp3<sup>+</sup>CD25<sup>+</sup>Tregs (\*\*\*\* $p$  = 0.0002) in 6 tumors (day 13) from WT or LT $\beta$ R<sup>-/-</sup> C57BL6 mice by flow cytometry **(m)**. **n** Lung colonization assessed at 3 weeks after tail vein injection of  $3 \times 10^5$  B16F10 cells with or without primary mouse LECs ( $1 \times 10^5$ ) to WT or LT $\beta$ R<sup>-/-</sup> C57BL6 mice ( $n = 8$  per group, five representative lung images per group shown). \*\* $p$  = 0.0023, \*\*\* $p$  = 0.0009. Representative of 3 **(a–c, e, f)** and 2 **(g–n)** independent experiments shown. **a–n** Mean  $\pm$  SEM. \*\*\*\* $p$  < 0.0001 by one-way ANOVA **(a–c, e, f, h, i, n)** or unpaired two-tailed  $t$ -test **(k, m)**. Source data are provided as a Source Data file.

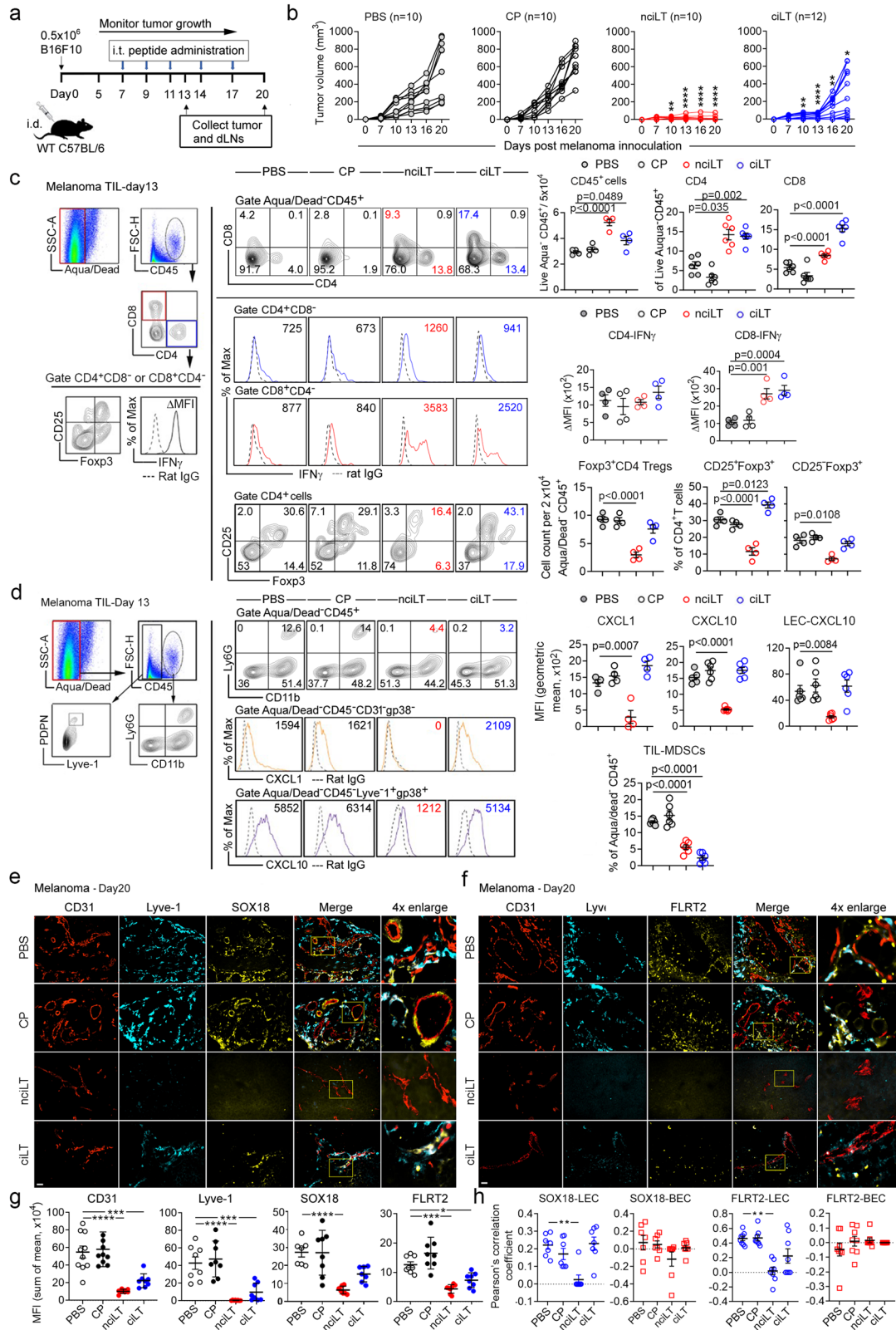
may relate to varied TRAF2 and TRAF3 associations with the LT $\beta$ R receptor in these cells. Conversely, activation of LT $\beta$ R promoted tumor TEM. Notably, the presence of LECs significantly promoted tumor cell migration, suggesting LEC-derived adhesion or junctional molecules and chemokines are critical. We also observed that blocking LT $\beta$ R-NIK signaling inhibited tumor cell growth and promoted apoptosis. Classical NF $\kappa$ B signaling is constitutively activated in tumor cells, yet ciLT did not affect tumor growth and produced modest inhibition of B16F10 TEM. LT $\beta$ R-depleted melanoma cells, in which the entire receptor signaling is ablated, had slower in vivo growth and lymphatic metastasis, although there was no defect in growth in vitro, implicating the importance of environmental cues or intercellular communication in the TME. RNA-seq analysis of LT $\beta$ R-depleted B16F10 revealed decreased gap junction protein GJA1, PDPN, NOTCH3, and BCAM1, which all regulate cell adhesion and may contribute to the reduced migration and metastasis. Thus, the complexities of LT $\beta$ R signaling likely account for the diverse effects of receptor blockade or activation. These observations suggest that a more specific approach, as we show here on LT $\beta$ R signaling pathways, may be more efficacious for tumor therapy.

We found Tregs use LT $\alpha$ 1 $\beta$ 2 to preferentially stimulate tumor LT $\beta$ R nonclassical NF $\kappa$ B-NIK signaling to enhance tumor growth and migration. In contrast, neither LT $\alpha$  knockout Tregs nor Teffs enhanced tumor growth or migration. To clarify the role of other related receptor-ligand interactions between Tregs and tumor cells, we analyzed the other ligand of LT $\beta$ R, LIGHT, however it was not detected on Tregs, while Teffs and B16F10 had negligible LIGHT expression (Supplementary Fig. 7a). Tregs have the highest level of HVEM, the receptor of LIGHT, while B16F10 has minimal HVEM expression, indicating Tregs and Teffs are unlikely to signal B16F10 through LIGHT/HVEM. Tregs but not LT $\alpha$ -deficient Tregs or Teffs induced melanoma LT $\beta$ R nonclassical NF $\kappa$ B signaling, which was selectively inhibited by nciLT, further evidence that other receptors and ligands of the LT $\beta$ R family are not involved. Other immune cells, such as B cells and CD8 T cells, also express LT $\alpha$ 1 $\beta$ 2, but the expression levels are less than that of Tregs in either homeostatic conditions or TME. Similar to Teffs, B cells did not induce LT $\beta$ R-nonclassical NF $\kappa$ B signaling and had no impact on tumor cell migration. Hence, Tregs are the major source of LT $\alpha$ 1 $\beta$ 2 to engage LT $\beta$ R on melanoma or breast cancer cells to promote tumor growth and TEM.

Adoptively transferred WT Tregs but not LT $\alpha$ -deficient Tregs promote tumor growth, and adoptively transferred primary LECs also restore tumor malignancy in LT $\beta$ R-deficient mice, indicating the critical roles of Treg LT $\alpha$ 1 $\beta$ 2–LT $\beta$ R interaction on tumor cells and LECs.

Since LT $\alpha$ -deficient Tregs had no defect in immune suppression and viability<sup>11</sup>, failure to suppress immunity was not the cause of their inability to promote tumor growth. Mechanistically, Treg-driven LT $\beta$ R nonclassical NF $\kappa$ B signaling stimulates both tumor and LEC responses that sustain tumor survival, growth, and metastases. In the tumor, this signaling drives expression of angiogenic and immunosuppressive myeloid chemokines CXCL1, CXCL10, and CCL5; protumor interferon-stimulated genes *ISG15* and *IFIT3*; and oncoprotein *USP18*, all of which promote tumor growth and metastases, and are selectively blocked by nciLT but not by ciLT. In LEC, this signaling drives endothelial-specific pro-lymphangiogenic SOX18, tumorigenic FLRT2, proangiogenic tumor endothelial molecules Clec14 and Apelin, and myeloid tropic chemokines to promote tumor growth and TEM. The Treg-activated LEC also directly favored tumor growth via cell-cell contact, and nciLT but not ciLT abolished this effect. Additionally, Treg LT $\alpha$ 1 $\beta$ 2 directly reduced LV and LEC junctional VE-cadherin expression to transform them from continuous “zipper” to discontinuous “button” junctions, promoting CD4 and CD8 egress from the tumor, thus impairing intratumoral immunity.

Leveraging in vivo Treg interactions with tumor and LECs, nciLT dramatically suppressed melanoma growth and metastasis with increased intratumoral IFN $\gamma$ <sup>+</sup>CD8 T cells and reduced tumor CD25<sup>+</sup>CD4<sup>+</sup> Tregs and MDSC infiltration and angiogenesis. Notably, nciLT reduced SOX18 and FLRT2 on tumor LECs, in line with SOX18-deficient mice having suppressed B16F10 lymphangiogenesis and metastases<sup>46</sup> and pharmaceutical inhibition of SOX18 reduced breast cancer vascularization and metastases<sup>47</sup>. FLRT2 on tumor endothelial cells forms homophilic interendothelial adhesions to safeguard against oxidative stress, and endothelium-specific deletion of FLRT2 suppressed tumor metastases<sup>35</sup>. Tumor and LEC-derived CXCL1 and CXCL10, recruit CXCR2<sup>+</sup>MDSCs<sup>48</sup> and CXCR3<sup>+</sup>Tregs<sup>49</sup> (Supplementary Fig. 7b), respectively. Thus, suppression of these chemokines by nciLT are likely key attributes for the reduced immune suppressive cells in tumor and enhanced anti-tumor immunity. Since CXCL10 recruits both Tregs and CD8 T cells<sup>50</sup>, blockade of the initial prompt recruitment of Tregs to the tumor bed may play a critical role in tumor regression, which unleashes CD8 proliferation in the TME. In addition to their chemotactic properties, CXCL1 is implicated in tumor growth, angiogenesis, and tumorigenesis<sup>51</sup>. ciLT also enhanced effector T cells and reduced MDSCs in TME, which may contribute to efficient tumor regression at the early stage. The absence of inhibitory effects of ciLT on the CXCLs chemokines may contribute to later tumor relapse. ciLT also suppressed tumor angiogenesis with less efficiency than nciLT. It is noteworthy that LT $\beta$ R-classical NF $\kappa$ B-driven *RPL21*, *RPL30*, *MIEN1*,



and *NR4a1*, are selectively inhibited by ciLT. These rapidly induced early response protumor genes are overexpressed in various human cancers and proposed as targets for tumor therapy<sup>51-53</sup>. Therefore, ciLT and nciLT combined therapy at selected times may optimize therapeutic efficacy. Together, our data revealed that Treg LT $\alpha\beta$  promotes LT $\beta$ R signaling in tumor cells and LECs. Selectively targeting Tregs or Treg-induced classical and nonclassical LT $\beta$ R-NF $\kappa$ B signaling on tumor

cells and LECs may provide a rational strategy to efficiently prevent tumor growth and metastasis.

## Methods

### Mice

Female C57BL/6J (WT, LT $\beta$ R<sup>-/-</sup>, LT $\alpha$ <sup>-/-</sup>) (7-10 weeks), were purchased from The Jackson Laboratory (Bar Harbor, ME). Foxp3GFP mice on a

**Fig. 7 | Blockade of LT $\beta$ R-nonclassical NF $\kappa$ B inhibits tumor growth, immune suppressive cell recruitment, and tumor angio- and lymphangiogenesis.**  
**a, b** Intradermally transferred B16F10 melanoma in C57BL/6 mice treated with an intratumoral or peritumoral injection of 10 nmol per tumor of nciLT, ciLT, or CP for 5 days. Scheme of tumor treatment (**a**). Tumor growth (**b**), ten mice in each cohort except for the nciLT-treated group ( $n = 12$ ).  $p$  values are calculated by comparing each peptide-treated group to the PBS group at days 7, 10, 13, 16, and 20 using an unpaired two-tail  $t$ -test. \*\*\*\* $p < 0.0001$ , \*\* $p = 0.0045$  (nciLT and ciLT day 10);  $p = 0.008$  (ciLT day 16), \* $p = 0.0405$ . **c, d** At day 13, tumors ( $n = 4$ ) analyzed for CD4, CD8, Foxp3<sup>+</sup> CD4 Tregs and T cell IFN $\gamma$  (**c**), Ly6G<sup>+</sup>CD11b<sup>+</sup> MDSCs, CXCL1, and CXCL10 expression in CD45<sup>+</sup> CD31<sup>+</sup>PDPN<sup>+</sup> cells or Lyve-1<sup>+</sup> PDPN<sup>+</sup> LECs (**d**) by flow

cytometry. Some samples were measured two more times in separate staining procedures to reach the accuracy (CD4, CD8, CXCL10, and MDSC). Gating strategy shown (**c, d**). **e, f** At day 20, tumors were assessed for angiogenesis (CD31<sup>+</sup>/Lyve-1<sup>+</sup>) and lymphangiogenesis (CD31<sup>+</sup>/Lyve-1<sup>+</sup>) by immunohistochemistry and analyzed for SOX18 (**e**) and FLRT2 (**f**). Representative of eight images of each group. Magnification 20x, scale bar:42  $\mu$ m. **g, h** Expression on CD31<sup>+</sup>/Lyve-1<sup>+</sup> lymphatic vessels and CD31<sup>+</sup>/Lyve-1<sup>+</sup> blood vessels of tumors ( $n = 5$ ). MFIs (**g**) and quantification of colocalization between SOX18 or FLRT2 and lymphatic or blood vessels (**h**). Representative of 2 (**a-h**) independent experiments shown. **c-h**: Mean  $\pm$  SEM. \* $p = 0.0116$ , \*\* $p = 0.0019$ , \*\*\* $p = 0.0005$ , \*\*\*\* $p < 0.0001$  by one-way ANOVA. Source data are provided as a Source Data file.

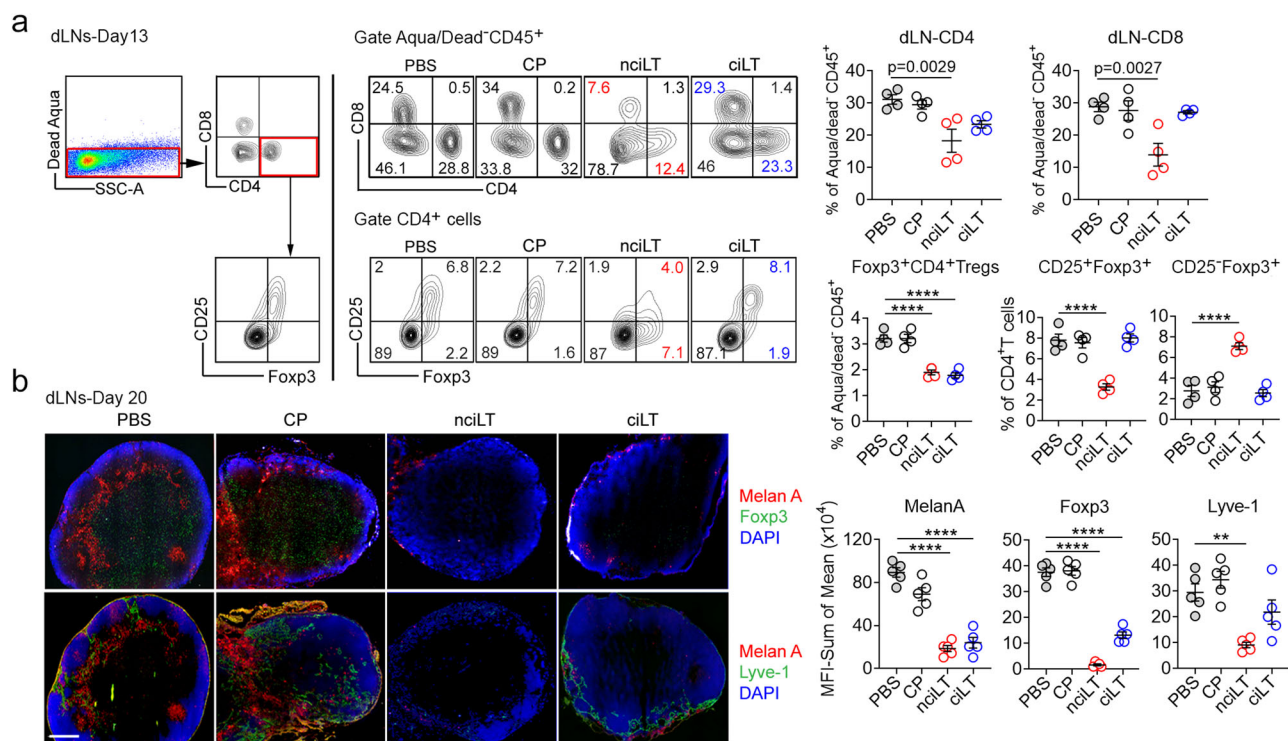


**Fig. 8 | Blockade of LT $\beta$ R-nonclassical NF $\kappa$ B signaling reduces CD4 Tregs in dLNs and suppresses melanoma lymphatic metastases.** **a, b** Same as in Fig. 7, B16F10 melanoma-bearing C57BL/6 mice treated with a peritumoral injection of 10 nmol/tumor of nciLT, ciLT, or CP for 5 days. At day 13, dLNs ( $n = 4$ ) analyzed for CD4, CD8, CD25<sup>+</sup>, or CD25<sup>-</sup> Foxp3<sup>+</sup> CD4 Tregs by flow cytometry (**a**). The gating

strategy is shown. Draining LNs ( $n = 5$  per group) at day 20 assessed for tumor metastasis (Melan-A), Tregs (Foxp3), and lymphangiogenesis (Lyve-1) by immunohistochemistry (**b**). Representative image with scale bar: 500  $\mu$ m. **a, b**. Representative of two independent experiments. Mean  $\pm$  SEM. \*\* $p = 0.0015$ , \*\*\*\* $p < 0.0001$  by one-way ANOVA. Source data are provided as a Source Data file.

C57BL/6 background were from Dr. A. Rudensky (Memorial Sloan Kettering Cancer Center) (Fontenot et al., 2005). LT $\alpha^{-/-}$  mice were crossed with Foxp3GFP mice to generate LT $\alpha^{-/-}$ Foxp3GFP mice. All animal experiments were performed in accordance with the Institutional Animal Care and Use Committee (IACUC) of the University of Maryland at Baltimore approved protocols. Animals of mixed sex and similar age were used within each cohort. The maximum allowable tumor size/burden (with a diameter of less than 2 cm) was not exceeded. Mice were housed at an ambient temperature of  $24 \pm 2$  °C, with circulating air, constant humidity of  $50 \pm 10\%$ , and a 12-h light/dark cycle.

### Cell lines

The mouse melanoma B16F10-eGFP and mouse breast cancer 4T1-eGFP from Imanis Life Sciences (Rochester, MN), B16F10 and Human melanoma A375 from the American Type Culture Collection, were cultured in DMEM with GlutaMAX (4.5 g/L glucose, Invitrogen) containing 10% FCS (Gemini, CA) and 1% Penicillin/

Streptomycin (Invitrogen). C57BL/6 mouse (C57-6064L) or human (H-6064L) primary dermal LECs were from Cell Biologics, Inc. (Chicago, IL), and were cultured according to the manufacturer's instructions in manufacturer-provided mouse endothelial cell medium supplemented with 5% FBS, 2 mM L-glutamine, 100 IU/mL penicillin, vascular endothelial growth factor, endothelial cell growth supplement, heparin, epidermal growth factor, and hydrocortisone.

### Peptides

LT $\beta$ R decoy peptides were synthesized by GenScript. All peptides were >95% purity, dissolved in endotoxin-free ultrapure water. Peptide reconstitution and usage were described previously<sup>3</sup>. Peptide sequences can be found in Supplementary Table 3.

### Mouse T cell and B cell purification and culture

Mouse naïve CD4 T and B cells were isolated using mouse CD4 and B cell negative selection kits (Stemcell Technologies, Cambridge, MA).



CD4<sup>+</sup>Foxp3GFP<sup>+</sup> Tregs or CD4<sup>+</sup>Foxp3<sup>-</sup> GFP<sup>-</sup> naïve CD4 T cells were sorted from total CD4 T cells from LNs and spleens of WT or LT $\alpha$ <sup>-/-</sup> Foxp3GFP mice using a FACS Aria II (BD Biosciences, San Jose, CA) with >98% purity. The sorted Tregs were cultured overnight at 37 °C in 5% CO<sub>2</sub>, with medium containing IL-2 (20 ng/mL, eBioscience, San Diego, CA), plate-bound anti-CD3 $\epsilon$  mAb (1  $\mu$ g/mL, clone 145-2C11, eBioscience), and anti-CD28 mAb (1  $\mu$ g/mL, clone 37.52, eBioscience), and human TGF $\beta$ 1 (10 ng/mL, eBioscience). For effector T cells, the sorted naïve CD4 T cells were cultured with the medium but without human TGF $\beta$ 1 for 3 days. All cells were cultured in complete RPMI 1640 supplemented with 10% FBS, 1 mM sodium pyruvate, 2 mM L-glutamine, 100 IU/mL penicillin, 100  $\mu$ g/mL streptomycin, non-essential amino acids, and 2  $\times$  10<sup>-5</sup> M 2-ME (Sigma-Aldrich).

### Human natural Treg and naïve CD4 T cell purification and activation

Human Tregs were enriched from peripheral blood mononuclear cells (purchased from Memorial Blood Center (St. Paul, MN), complying with all relevant ethical regulations, donor consents, and Institutional Review Board (IRB) of Memorial Blood Center approval or exemption (<https://www.mbc.org/products-and-services/research/>)) with anti-CD25 microbeads (Miltenyi Biotec, Bergisch Gladbach, Germany). The CD4<sup>+</sup>CD25<sup>high</sup>CD127<sup>-</sup>CD45RA<sup>+</sup> natural Treg (nTreg) and CD4<sup>+</sup>CD25<sup>-</sup>CD127<sup>+</sup>CD45RA<sup>+</sup> naïve CD4 T cells were sorted by flow cytometry and were expanded as previously described<sup>54</sup>. Briefly, purified nTreg were stimulated with irradiated KT64/86 cells cultured in XVivo-15 (BioWhittaker, Walkersville, MD) media containing 10% human AB serum (Valley Biomedical, Winchester, VA), Pen/Strep (Invitrogen, Carlsbad, CA), N-acetyl cysteine (USP), and recombinant IL-2 (300 IU/mL; Chiron, Emeryville, CA) for 14 days and frozen. The frozen nTreg and naïve CD4 were thawed and re-stimulated with anti-CD3/CD28 mAb-Dynabeads (Life Technologies, Carlsbad, CA) at 1:3 (cell to bead) plus recombinant IL-2 (300 U/mL) for 10 days before assay.

### MTT viability assay and cell apoptosis analysis

Cells were plated into 24-well tissue culture plates. After treatment, the cells were washed and followed by 3-h incubation with 0.5 mg/mL MTT (3-(4, 5-Dimethylthiazol-2-yl)-2,5 diphenyl tetrazolium bromide) (Sigma-Aldrich). Cell apoptosis was measured with Annexin V Apoptosis Detection Kit I (BD Pharmingen) following manufactory instructions.

### Flow cytometry

Cells were washed and incubated with anti-CD16/32 (clone 93, eBioscience), followed by incubation with fluorescently labeled antibodies (See Supplementary Table 3) for 30 min at 4 °C. Cells were then washed and fixed with 4% paraformaldehyde. Data acquisition was performed using an LSR Fortessa flow cytometer (BD Biosciences) and analyzed with FlowJo 10. 8.1 (Tree Star, Inc).

### Immunoblotting

Cells were lysed in buffer containing 20 mM Hepes (pH 7.4), 150 mM NaCl, 10 mM NaF, 2 mM Na<sub>3</sub>VO<sub>4</sub>, 1 mM EDTA, 1 mM EGTA, 0.5% Triton X-100, 0.1 mM DTT, 1 mM PMSF, and protease inhibitor cocktail (Roche). Protein in the cell extract was quantified using a protein quantification kit (Bio-Rad, Philadelphia, PA), and 10  $\mu$ g total protein was run on Novex™ WedgeWell™ 4–20% Tris-Glycine Mini Gels (Invitrogen) and transferred to an Immobilon-P membrane (Bio-Rad). Membranes were probed with indicated antibodies (See Supplementary Table 3). Quantification of blots was performed with ImageJ from the National Institutes for Health. The relative intensity of blots was normalized to housekeeping gene GAPDH and presented as fold induction to non-stimulation.

### Quantitative reverse transcription PCR and cDNA microarray analysis

About 1  $\mu$ g of total RNA extracted using Trizol reagent (Invitrogen) was reverse transcribed into cDNA with GoScript™ Reverse Transcription System (Promega, Fitchburg, WI). mRNA expression levels were quantified by real-time PCR using SYBR Green Master Mix with an ABI Prism 7900HT (Applied Biosystems, Foster City, CA). Values for specific gene expression were normalized to housekeeping HPRT gene expression and were calculated as: 2<sup>-(Ct of HPRT–Ct specific gene)</sup>. For microarray analysis, samples were further cleaned using an RNeasy Mini Kit (QIAGEN), labeled with Cyanine 3-CTP using a Low Input Quick Amp Labeling Kit (Agilent), and hybridized to a SurePrint G3 Mouse GE Microarray (Agilent). Fluorescence was scanned using a DNA Microarray Scanner (Agilent) and quantified with Feature Extraction ver 10.7.1.1 (Agilent). Expression values for each probe set were calculated using the RMA method with GeneSpring Gx 12.0 software (Agilent). Primers can be found in Supplementary Table 3.

### Bulk RNA sequencing

Total RNA was isolated using the NucleoSpin RNA Plus kit per the manufacturer's instructions. Messenger RNA was purified and sequenced by Novogene. Reference genome and gene model annotation files were downloaded from Ensembl directly. Index of the reference genome was built using Hisat2 v2.0.5 and paired-end clean reads were aligned to the reference genome using Hisat2 v2.0.5. featureCounts v1.5.0-p3 was used to count the reads numbers mapped to each gene. FPKM (fragments per kilobase of transcript sequence per millions) of each gene was calculated based on the length of the gene and the read count mapped to this gene. Differential expression analysis of two conditions was performed using the edgeR R package (version 3.22.5). Differential expression analysis of two conditions/groups (two biological replicates per condition) was performed using the DESeq2 R package (1.20.0). The resulting *P*-values were adjusted using Benjamini and Hochberg's approach for controlling the false discovery rate. Genes with an adjusted *P* value  $\leq$  0.05 found by DESeq2 were assigned as differentially expressed. Gene ontology (GO) enrichment analysis of differentially expressed genes was implemented by the clusterProfiler R package.

### Time-lapse microscopy

WT or LT $\beta$ R<sup>-/-</sup>BI6F10-GFP (5  $\times$  10<sup>4</sup> cells per transwell) migrating across endothelial monolayers to CCL19 (50 ng/mL) were visualized by EVOS FL Auto Cell Imaging System (Thermo Fisher Scientific) with a  $\times$ 20 objective. One image was captured every 5 min for 3 h. Cell tracks were analyzed with Volocity version 6.3 software (Perkin Elmer).

### Tumor cell lymphatic transendothelial migration

Transmigrations across endothelial cells were described previously (ref. 11; ref. 22). Briefly, the inverted transwell insert (24-well, Corning International) with 8  $\mu$ m pore size was coated with 0.2% (w/v) gelatin (Bio-Rad) for 1 h at 37 °C before loading with 1.0  $\times$  10<sup>5</sup> primary skin LEC in 100  $\mu$ L LEC medium. After 2 days, the LEC cell layers were treated with various conditions as noted in the text and figure legends prior to adding 1  $\times$  10<sup>5</sup> tumor cells in 100  $\mu$ L to the upper chamber of the transwell plate while the lower chamber contained SIP (Avanti Polar Lipids, Inc., Alabaster, AL). All cells or reagents were prepared in IMDM containing transferrin and 0.5% (w/v) fatty acid-free BSA (Gemini, West Sacramento, CA). T cells that migrated to the lower chamber after 3 h at 37 °C were counted.

### Cell migration assay

The cells were seeded in a 12-well plate and cultured to 90% confluence. The plates were scratched with a sterile 200  $\mu$ L pipette tip on the cell monolayer. The cells pretreated with peptides were then

cultured for 48 h. The images were acquired using an ordinary optics microscope (Olympus, Japan) at 0 and 48 h. The migration percentage was calculated according to this formula: (the size of the cell defect at 0 h – the size of the defect at 48 h)/the size of the defect at 0 h.

### Immunohistochemistry

Cell monolayers or tissues were fixed for 20 min at 4 °C with 4% (w/v) paraformaldehyde (Affymetrix, Santa Clara, CA), then permeabilized with PBS 0.2% (v/v) Triton X-100 (Sigma-Aldrich) and treated with 4% donkey serum for 30 min then incubated with primary antibodies (see Supplementary Table 3) for overnight at 4 °C. The bound antibodies were detected with Alexa Fluor 448, 647 (Cy5), or 546 (Cy3)-conjugated secondary antibodies (Jackson ImmunoResearch, West Grove, PA) for 1 h at 4 °C. The mounted slides were visualized by fluorescent microscopy (Zeiss LSM 510 Meta and LSM5 Duo). Images were analyzed with Volocity version 6.3 software. Quantification of the junctional VE-cadherin in 60x magnified images of LVs of whole-mounted LVs or adherent LECs was performed with ImageJ. Length of zipper junctions and button junctions were measured. The percentage of zipper junction was calculated as the length of zipper junction  $\times$  100/ (length of zipper junction + length of button junction)<sup>55</sup>.

### CRISPR/Cas9 knockout of LT $\beta$ R, NIK, and IKK $\beta$ in B16F10 and LECs

gRNA designed to target the common exons for all murine LT $\beta$ R, NIK, and IKK $\beta$  isoforms were synthesized as oligo: 5'-AGCCGAGTGCCGCTGTCAGC-3', 5'-GCTGGCCGCATCAAGGTTA-3', and 5'-CGCCATCAA GCAATGCCGAC-3', respectively and cloned to lentiCRISPRv2 (include Cas9 and puromycin-resistant gene) vector by GenScript. Lentiviruses were produced by co-transfecting HEK293T cells with the packaging plasmids psPAX2 and pMD2.G (Addgene plasmid # 12260 and 12259) and the transfer plasmid lentiCRISPRv2-gRNAs, using Lipofectamine 2000 (Thermo Fisher Scientific). The media was changed to antibiotic-free complete DMEM with 10% FBS after 16 h. The lentivirus supernatants were collected 24 and 48 h after transfection and filtered through 0.45 mm PES syringe filter (SARSTEDT, Newton, NC). mLEC, B16F10, or B16F10-fluc/eGFP were transduced with the lentiviruses for 3 days, followed by a selection medium containing 2 mg/mL puromycin (Sigma-Aldrich) for 3 days. LT $\beta$ R-lentiCRISPRv2 transduced B16F10-fluc/eGFP cells which have Neomycin and Puromycin resistance, were flow sorted for GFP<sup>+</sup>LT $\beta$ R<sup>-</sup> cells. Surviving or sorted cells were expanded and checked with immunoblotting of NIK and IKK $\beta$  expression or flow cytometry analysis of LT $\beta$ R surface expression.

### Tumor treatments

WT or LT $\beta$ R<sup>-/-</sup> C57/BL6J mice (7–8 weeks old, female) were subcutaneously injected with  $0.5 \times 10^6$  WT B16F10 or B16F10-fluc/eGFP tumor cells. 5, 7, 9, and 11 days after tumor inoculation, tumor-bearing mice were peritumoral injected with 20 nmol of CP, nciLT, or ciLT. The tumor volume was recorded for each mouse every 2 days and calculated according to (longest width)  $\times$  (longest length)<sup>2</sup>/2. 2 or 9 days after the last peptide treatment, six mice from each group were euthanized, and the tumors and dLNs were harvested and analyzed by flow cytometry or immunohistochemistry. Parallel groups of mice were monitored daily for tumor growth. There were 6 to 10 mice in each group. For the Treg adoptive transfer assay, induced Tregs differentiated from naïve CD4 T cells from WT or LT $\alpha$  KO Foxp3GFP transgenic mice were FACS sorted before intravenous transfer of  $0.5 \times 10^6$  cells per mouse. For the LEC adoptive transfer assay,  $1 \times 10^5$  primary mouse LECs were intravenously transferred to WT or LT $\beta$ RKO C57BL/6 mice inoculated with WT B16F10. For the pulmonary metastases study, mice were injected via the tail vein with  $0.3 \times 10^6$  WT B16F10 or B16F10-fluc/eGFP. Lungs were harvested on day 21 after injection.

### Quantification and statistical analysis

Numerical data are presented as mean  $\pm$  SEM. Asterisks mark data statistically different from the controls, with *p* values noted in the figure legends. The *p* values were calculated by one-way or two-way ANOVA and Student's *t*-tests (paired or unpaired) using GraphPad Prism version 10.1.0 (La Jolla, CA). The number of replicates is noted in the figure legends.

### Reporting summary

Further information on research design is available in the Nature Portfolio Reporting Summary linked to this article.

### Data availability

The RNA sequencing data and cDNA microarray processed data generated in this study has been deposited and have been made publicly available at NCBI's Gene Expression Omnibus (GEO) repository with accession numbers [GSE271338](https://www.ncbi.nlm.nih.gov/geo/query/acc.cgi?acc=GSE271338) and [GSE270960](https://www.ncbi.nlm.nih.gov/geo/query/acc.cgi?acc=GSE270960), respectively. The TCGA data of human skin cutaneous melanoma, breast cancer, lung cancer patients were accessible using the NIH-NCI GDC Data Portal (<https://portal.gdc.cancer.gov/>)<sup>56</sup> using the following accessions: skin cutaneous (phs000178), melanoma, breast cancer (phs000178), and lung cancer (phs000178) [[https://www.ncbi.nlm.nih.gov/projects/gap/cgi-bin/study.cgi?study\\_id=phs000178](https://www.ncbi.nlm.nih.gov/projects/gap/cgi-bin/study.cgi?study_id=phs000178)]. The remaining data were available within the Article, Supplementary Information or Source Data file. Source data are provided with this paper.

### References

- Lukashev, M. et al. Targeting the lymphotoxin-beta receptor with agonist antibodies as a potential cancer therapy. *Cancer Res.* **66**, 9617–9624 (2006).
- Gommerman, J. L. & Browning, J. L. Lymphotoxin/light, lymphoid microenvironments and autoimmune disease. *Nat. Rev. Immunol.* **3**, 642–655 (2003).
- Piao, W. et al. Regulation of T cell afferent lymphatic migration by targeting LTbetaR-mediated non-classical NFkappaB signaling. *Nat. Commun.* **9**, 3020 (2018).
- Wolf, M. J., Seleznik, G. M., Zeller, N. & Heikenwalder, M. The unexpected role of lymphotoxin beta receptor signaling in carcinogenesis: from lymphoid tissue formation to liver and prostate cancer development. *Oncogene* **29**, 5006–5018 (2010).
- Keats, J. J. et al. Promiscuous mutations activate the noncanonical NF-kappaB pathway in multiple myeloma. *Cancer Cell* **12**, 131–144 (2007).
- Hehlgans, T. et al. Lymphotoxin-beta receptor immune interaction promotes tumor growth by inducing angiogenesis. *Cancer Res.* **62**, 4034–4040 (2002).
- Tang, H. et al. Facilitating T cell infiltration in tumor microenvironment overcomes resistance to PD-L1 blockade. *Cancer Cell* **30**, 500 (2016).
- Hu, X. et al. Lymphotoxin beta receptor mediates caspase-dependent tumor cell apoptosis in vitro and tumor suppression in vivo despite induction of NF-kappaB activation. *Carcinogenesis* **34**, 1105–1114 (2013).
- Kos, K. et al. Tumor-educated T(regs) drive organ-specific metastasis in breast cancer by impairing NK cells in the lymph node niche. *Cell Rep.* **38**, 110447 (2022).
- Kos, K. & de Visser, K. E. The multifaceted role of regulatory T cells in breast cancer. *Annu. Rev. Cancer Biol.* **5**, 291–310 (2021).
- Brinkman, C. C. et al. Treg engage lymphotoxin beta receptor for afferent lymphatic transendothelial migration. *Nat. Commun.* **7**, 12021 (2016).
- Piao, W. et al. Regulatory T cells condition lymphatic endothelia for enhanced transendothelial migration. *Cell Rep.* **30**, 1052–1062 e1055 (2020).

13. Onder, L. et al. Endothelial cell-specific lymphotoxin-beta receptor signaling is critical for lymph node and high endothelial venule formation. *J. Exp. Med.* **210**, 465–473 (2013).
14. Zhai, Y. et al. LIGHT, a novel ligand for lymphotoxin beta receptor and TR2/HVEM induces apoptosis and suppresses in vivo tumor formation via gene transfer. *J. Clin. Invest.* **102**, 1142–1151 (1998).
15. Leong, S. P., Naxerova, K., Keller, L., Pantel, K. & Witte, M. Molecular mechanisms of cancer metastasis via the lymphatic versus the blood vessels. *Clin. Exp. Metastasis* **39**, 159–179 (2022).
16. Kohli, K., Pillarisetty, V. G. & Kim, T. S. Key chemokines direct migration of immune cells in solid tumors. *Cancer Gene Ther.* **29**, 10–21 (2022).
17. Yang, H. et al. Sox17 promotes tumor angiogenesis and destabilizes tumor vessels in mice. *J. Clin. Invest.* **123**, 418–431 (2013).
18. Grimm, D. et al. The role of SOX family members in solid tumours and metastasis. *Semin Cancer Biol.* **67**, 122–153 (2020).
19. Chen, H., Xu, C., Jin, Q. & Liu, Z. S100 protein family in human cancer. *Am. J. Cancer Res.* **4**, 89–115 (2014).
20. Acharyya, S. et al. A CXCL1 paracrine network links cancer chemoresistance and metastasis. *Cell* **150**, 165–178 (2012).
21. Cartier, A. & Hla, T. Sphingosine 1-phosphate: lipid signaling in pathology and therapy. *Science* <https://doi.org/10.1126/science.aar5551> (2019).
22. Xiong, Y. et al. A robust in vitro model for trans-lymphatic endothelial migration. *Sci. Rep.* **7**, 1633 (2017).
23. Wang, N. et al. CXCL1 derived from tumor-associated macrophages promotes breast cancer metastasis via activating NF-kappaB/SOX4 signaling. *Cell Death Dis.* **9**, 880 (2018).
24. Kim, M., Choi, H. Y., Woo, J. W., Chung, Y. R. & Park, S. Y. Role of CXCL10 in the progression of in situ to invasive carcinoma of the breast. *Sci. Rep.* **11**, 18007 (2021).
25. Aldinucci, D. & Colombatti, A. The inflammatory chemokine CCL5 and cancer progression. *Mediators Inflamm.* **2014**, 292376 (2014).
26. Bolado-Carrancio, A. et al. ISGylation drives basal breast tumour progression by promoting EGFR recycling and Akt signalling. *Oncogene* **40**, 6235–6247 (2021).
27. Pidugu, V. K., Pidugu, H. B., Wu, M. M., Liu, C. J. & Lee, T. C. Emerging functions of human IFIT proteins in cancer. *Front. Mol. Biosci.* **6**, 148 (2019).
28. Hong, B. et al. USP18 is crucial for IFN-gamma-mediated inhibition of B16 melanoma tumorigenesis and antitumor immunity. *Mol. Cancer* **13**, 132 (2014).
29. Kang, J. et al. Ribosomal proteins and human diseases: molecular mechanisms and targeted therapy. *Signal Transduct. Target Ther.* **6**, 323 (2021).
30. Kpetemey, M. et al. MIEN1, a novel interactor of Annexin A2, promotes tumor cell migration by enhancing Anx2 cell surface expression. *Mol. Cancer* **14**, 156 (2015).
31. Hibino, S. et al. Inhibition of Nr4a receptors enhances antitumor immunity by breaking Treg-mediated immune tolerance. *Cancer Res.* **78**, 3027–3040 (2018).
32. Sidibe, A. & Imhof, B. A. VE-cadherin phosphorylation decides: vascular permeability or diapedesis. *Nat. Immunol.* **15**, 215–217 (2014).
33. Futterer, A., Mink, K., Luz, A., Kosco-Vilbois, M. H. & Pfeffer, K. The lymphotoxin beta receptor controls organogenesis and affinity maturation in peripheral lymphoid tissues. *Immunity* **9**, 59–70 (1998).
34. Young, N. et al. Effect of disrupted SOX18 transcription factor function on tumor growth, vascularization, and endothelial development. *J. Natl Cancer Inst.* **98**, 1060–1067 (2006).
35. Ando, T. et al. Tumor-specific interendothelial adhesion mediated by FLRT2 facilitates cancer aggressiveness. *J. Clin. Invest.* <https://doi.org/10.1172/JCI153626> (2022).
36. Olbromski, M., Podhorska-Okolow, M. & Dziegiel, P. Role of the SOX18 protein in neoplastic processes. *Oncol. Lett.* **16**, 1383–1389 (2018).
37. Petersen, R. P. et al. Tumor infiltrating Foxp3+ regulatory T-cells are associated with recurrence in pathologic stage I NSCLC patients. *Cancer* **107**, 2866–2872 (2006).
38. Saleh, R. & Elkord, E. Acquired resistance to cancer immunotherapy: role of tumor-mediated immunosuppression. *Semin Cancer Biol.* **65**, 13–27 (2020).
39. Ring, S. et al. Regulatory T cells prevent neutrophilic infiltration of skin during contact hypersensitivity reactions by strengthening the endothelial barrier. *J. Invest. Dermatol.* **141**, 2006–2017 (2021).
40. He, M. X. et al. Transcriptional mediators of treatment resistance in lethal prostate cancer. *Nat. Med.* **27**, 426–433 (2021).
41. Wu, S. Z. et al. A single-cell and spatially resolved atlas of human breast cancers. *Nat. Genet.* **53**, 1334–1347 (2021).
42. Wu, S. Z. et al. Cryopreservation of human cancers conserves tumour heterogeneity for single-cell multi-omics analysis. *Genome Med.* **13**, 81 (2021).
43. Zilionis, R. et al. Single-cell transcriptomics of human and mouse lung cancers reveals conserved myeloid populations across individuals and species. *Immunity* **50**, 1317–1334 e1310 (2019).
44. Daller, B. et al. Lymphotoxin-beta receptor activation by lymphotoxin-alpha(1)beta(2) and LIGHT promotes tumor growth in an NFkappaB-dependent manner. *Int. J. Cancer* **128**, 1363–1370 (2011).
45. Das, R. et al. Lymphotoxin-beta receptor-NIK signaling induces alternative RELB/NF-kappaB2 activation to promote metastatic gene expression and cell migration in head and neck cancer. *Mol. Carcinog.* **58**, 411–425 (2019).
46. Duong, T. et al. Genetic ablation of SOX18 function suppresses tumor lymphangiogenesis and metastasis of melanoma in mice. *Cancer Res.* **72**, 3105–3114 (2012).
47. Overman, J. et al. Pharmacological targeting of the transcription factor SOX18 delays breast cancer in mice. *Elife* <https://doi.org/10.7554/eLife.21221> (2017).
48. Highfill, S. L. et al. Disruption of CXCR2-mediated MDSC tumor trafficking enhances anti-PD1 efficacy. *Sci. Transl. Med.* **6**, 237ra267 (2014).
49. Moreno Ayala, M. A. et al. CXCR3 expression in regulatory T cells drives interactions with type I dendritic cells in tumors to restrict CD8(+) T cell antitumor immunity. *Immunity* **56**, 1613–1630 e1615 (2023).
50. Ozga, A. J., Chow, M. T. & Luster, A. D. Chemokines and the immune response to cancer. *Immunity* **54**, 859–874 (2021).
51. Kushwaha, P. P., Gupta, S., Singh, A. K. & Kumar, S. Emerging role of migration and invasion enhancer 1 (MIEN1) in cancer progression and metastasis. *Front. Oncol.* **9**, 868 (2019).
52. Guo, H. et al. NR4A1 regulates expression of immediate early genes, suppressing replication stress in cancer. *Mol. Cell* **81**, 4041–4058 e4015 (2021).
53. Li, C. et al. RPL21 siRNA blocks proliferation in pancreatic cancer cells by inhibiting DNA replication and inducing G1 arrest and apoptosis. *Front. Oncol.* **10**, 1730 (2020).
54. Hippen, K. L. et al. Generation and large-scale expansion of human inducible regulatory T cells that suppress graft-versus-host disease. *Am. J. Transpl.* **11**, 1148–1157 (2011).
55. Zhang, F. et al. Lacteal junction zipper protects against diet-induced obesity. *Science* **361**, 599–603 (2018).
56. Grossman, R. L. et al. Toward a shared vision for cancer genomic data. *N. Engl. J. Med.* **375**, 1109–1112 (2016).

## Acknowledgements

This work was supported by NIH grant R37 AI062765 to J.S.B., Emerald grant 2022 to J.S.B. and W.P., R01 AI126596 and R01 HL141815 to R.A., R37 AI34495, R01 HL1879, R01 HL15514, and P01 CA 065493 to B.R.B. and K.L.H. Dr. Xiaoxuan Fan from UMB-Flow Core Facility for his excellent help for flow cell sorting and data analysis.



## Author contributions

W.P. and J.S.B. designed the research. W.P., L.W., Y.X., G.C.Z., S.M.P., M.L.S., R.S.O., J.S., K.H., C.M.P., D.K., Y.L., A.K., L.L., A.A., V.S., and M.W.S. performed the experiments. A.C.S. and Y.S. performed bioinformatic data analysis of the TCGA datasets. W.P., J.S.B., B.R.B., K.L.H., R.A., P.I., J.H.B., and C.M.J. analyzed and discussed the results. W.P. and J.S.B. wrote the manuscript.

## Competing interests

J.S.B., W.P., and X.Y. are inventors on a patent related to LT $\beta$ R antagonists entitled “Inhibitors of LT $\beta$ R-NF $\kappa$ B signaling pathways for treating inflammation and cancer” (Patent number: 11590202). The remaining authors declare no competing interests.

## Additional information

**Supplementary information** The online version contains supplementary material available at <https://doi.org/10.1038/s41467-024-54874-y>.

**Correspondence** and requests for materials should be addressed to Wenji Piao or Jonathan S. Bromberg.

**Peer review information** *Nature Communications* thanks the anonymous reviewer(s) for their contribution to the peer review of this work. A peer review file is available.

**Reprints and permissions information** is available at <http://www.nature.com/reprints>

**Publisher’s note** Springer Nature remains neutral with regard to jurisdictional claims in published maps and institutional affiliations.

**Open Access** This article is licensed under a Creative Commons Attribution-NonCommercial-NoDerivatives 4.0 International License, which permits any non-commercial use, sharing, distribution and reproduction in any medium or format, as long as you give appropriate credit to the original author(s) and the source, provide a link to the Creative Commons licence, and indicate if you modified the licensed material. You do not have permission under this licence to share adapted material derived from this article or parts of it. The images or other third party material in this article are included in the article’s Creative Commons licence, unless indicated otherwise in a credit line to the material. If material is not included in the article’s Creative Commons licence and your intended use is not permitted by statutory regulation or exceeds the permitted use, you will need to obtain permission directly from the copyright holder. To view a copy of this licence, visit <http://creativecommons.org/licenses/by-nc-nd/4.0/>.

© The Author(s) 2024